Appendix A

Gaussian Beam Propagation

In general, the light emitted from the laser can be approximated by assuming that the laser beam has an ideal Gaussian intensity profile, which corresponds to the theoretical TEM_{00} mode. In TEM_{00} mode, the beam coupled from a laser begins as a perfect plane wave with a Gaussian transverse irradiance profile as shown in Fig. B.1. To specify and discuss the propagation characteristics of a laser beam, it has to define its diameter at which the beam irradiance has fallen to $1/e^2$ of its peak, or axial value and the other define is the diameter at which the beam irradiance has fallen to 50% of its peak refereed as FWHM or full width at half maximum.

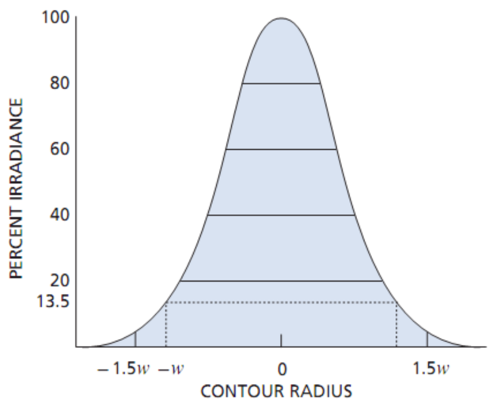

Fig. A.1: Irradiance profile of a Gaussian TEM_{00} mode

When the light wave propagates further, it becoming spread transversely caused by diffraction, and it is therefore impossible to have a perfectly collimated beam. The spreading of a laser beam can be predicated precisely from the pure diffraction theory; aberration is totally insignificant in the present context. Even, if a Gaussian TEM_{00} laser beam wavefront was perfect flat at some plane; it can quickly acquire curvature and begin spreading in accordance with

$$R(z) = z\left(1 + \left(\frac{\pi w_0^2}{\lambda z}\right)^2\right) \quad \text{(A-1)}$$

and $$w(z) = w_0\left(1 + \left(\frac{\lambda z}{\pi w_0^2}\right)^2\right)^{1/2} \quad \text{(A-2)}$$

where z is the distance propagated from the plane where the wavefront is flat, λ is the wavelength of light, w_0 is the radius of the $1/e^2$ irradiance contour at the plane where the wavefront is flat, $w(z)$ is the radius of the $1/e^2$ contour after the wave has propagated a distance a, and $R(z)$ is the wavefront radius of curvature after propagating a distance z. $R(z)$ is infinite at z=0, passes through a minimum at some finite z, and rises again towards infinity as z is further increased, asymptotically approaching the value of z itself. The plane z=0 marks the location of a Gaussian waist, or a place where the wavefront is flat and w_0 is called the beam waist radius.

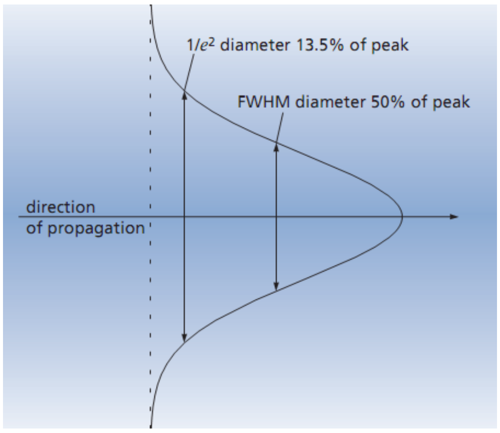

Fig. A.2: Diameter of a Gaussian beam

The irradiance distribution of the Gaussian TEM_{00} beam, namely,

$$I(r)=I_0e^{-2r^2/w^2}=\frac{2P}{\pi w^2}e^{-2r^2/w^2} \qquad \text{(A-3)}$$

where $w=w(z)$ and P is the total power in the beam, is the same at all cross section of the beam. Simultaneously, as $R(z)$ asymptotically approaches z for large z, $w(z)$ asymptotically approaches the value

$$w(z)=\frac{\lambda z}{\pi w_0} \qquad \text{(A-4)}$$

where$z$ is presumed to be much larger than $\pi w_0/\lambda$ so that the $1/e^2$ irradiance contours asymptotically approach a cone of angular radius

$$\theta=\frac{w(z)}{z}=\frac{\lambda}{\pi w_0} \qquad \text{(A-5)}$$

This value is the far-field angular radius of the Gaussian TEM_{00} beam. The vertex of the cone lies at the center of the waist, as shown in Fig.A.3.

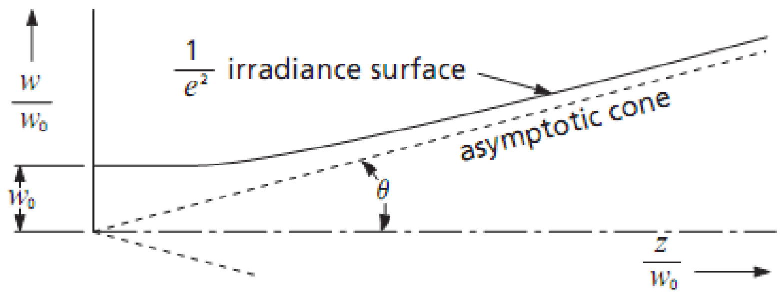

Fig. A.3: Growth in $1/e^2$ radius with distance propagated away from Gaussian waist

Thus, it is important to note that for a given value of λ, various of beam diameter and divergence with distance z are functions of a single parameter, w_0, the beam waist radius. Near the beam waist, the Gaussian beam is typically close to the output of the laser, the divergence angle is extremely small; far from the waist, the divergence angle approaches the asymptotic limit described above. The Raleigh range z_R defined as the distance over which the beam radius spreads by a factor of $\sqrt{2}$, is given by,

$$z_R = \frac{\pi w_0^2}{\lambda} \quad \text{(A-6)}$$

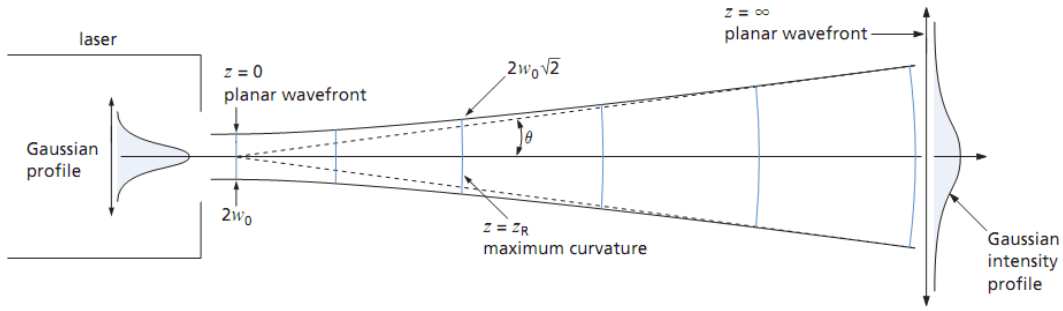

Fig. A.4: Change in wavefront radius with propagation distance

At the beam waist (z=0), the wavefront is planar. Likewise, at $z = \infty$, the wavefront is planar. As the beam propagates from the waist, the wavefront curvature must increase to a maximum and then begin to decrease, as shown in Fig. A.4. The Raleigh range considered to be the dividing line between near-field divergence and mid-range divergence, is the distance from the waist at which the wavefront curvature is a maximum. Far-field divergence must be measured at a distance much longer than z_R (usually>10*z_R). It is very important distinctions because calculations for spot size and other parameters in an optical train will be inaccurate if near or mid-field divergence values are used. For a tightly focused beam, the distance from the waist (the focal point) to the far-field can be few millimeters or less. For beams coming from the laser directly, the far-field distance can be measured in meters.

Normally, one has a fixed value for w_0 and uses the expression Eq. (A-2) to calculate the $w(z)$ for an input value of z. However, one can also using this equation to see how final beam radius varies with starting beams radius at a fixed distance z.

References

[1]. A. Siegman, Laser (Sausalito, CA: University Science Books, (1986).

[2]. S. A. Self, "Focusing of spherical Gaussian beams," Appl. Opt. 22, 5, 658, (1983).

[3]. H. Sun, "thin lens equation fir a real laser beam with weak lens aperture truncation," Opt. eng. 37, (1998).

[4]. R. J. Freiberg, A. S. Halsted, "Propagaties of low order transverse modes in argon ion lasers," Appl. Opt. 8, 355-362, (1963).

[5]. M. Born, E. Wolf, "Principle of optics" Seventh edition, (Cambridge, UK, 1999)

Appendix B

List of Published Papers

1. H. Z. Yang, S. W. Harun and H. Ahmad, "Fiber Optic Displacement and Liquid Refractive Index Sensors with Two Asymmetrical Inclined Fibers" Sensor and Transducer, September, (2009), Vol.108, pp.80-88.
2. K. S. Lim, S. W. Harun, H. Z. Yang, K. Dimyati, H. Ahmad, "Analytical and experimental studies on asymmetric bundle fiber displacement sensors" J. of Modern Optics, October (2009), Vol. 56, pp.1838-1842.
3. S. W. Harun, H. Z. Yang, M. Yasin, H. Ahmad, "Theoretical and experimental study on the fiber optic displacement sensor with two receiving fibers" Microwave and Optic technology Letters, Vol.52, pp.373-375, (2009).
4. H. Z. Yang, S. W. Harun, H. Ahmad, "Displacement sensing with two asymmetrical inclined fibers", Microwave and Optical Technology Letters, Vol. 52 Issue 6, pp. 1271 – 1274, (2010).
5. H. Z. Yang, K. S. Lim, S. W. Harun, H. Ahmad, "Enhanced bundle fiber displacement sensor based on concave mirror" Sensors and Actuators A, 162, 8-12, (2010).
6. S. W. Harun, M. Yasin, H. Z. Yang, Kusminarto, Karyono and H. Ahmad, "Estimation of Metal Surface Roughness Using Fiber Optic Displacement Sensor"

Laser Physics, Vol. 20, pp.1-6, (2010).

7. S.W. Harun, H.Z. Yang, H. Ahmad, "Theoretical and experimental studies on liquid refractive index sensor based on bundle fiber", Sensor Review, Vol. 31 Iss: 2, pp.173 – 177, (2011).

8. H.Z. Yang, S.W. Harun, H. Ahmad, "Theoretical and experimental studies on concave mirror-based fiber optic displacement sensor", Sensor Review, Vol. 31 Iss: 1, pp.65 – 69, (2011).

9. M. Yasin, S.W. Harun, H.Z. Yang, H. Ahma, “Fiber optic displacement sensor for measurement of glucose concentration in distilled water,” Optoelectronics and Advanced Materials-Rapid Comm. Vol. 4, Issue 8, (2010).

10. Yang, H. Z., Harun, S. W., Arof, H. and Ahmad, H., “Environment-independent liquid level sensing based on fiber-optic displacement sensors”. Microwave and Optical Technology Letters, 53: 2451–2453, (2011).

Sensors and Actuators A 162 (2010) 8–12

Contents lists available at ScienceDirect

Sensors and Actuators A: Physical

journal homepage: www.elsevier.com/locate/sna

Enhanced bundle fiber displacement sensor based on concave mirror

H.Z. Yang[a], K.S. Lim[a], S.W. Harun[a,b,*], K. Dimyati[b], H. Ahmad[a]

[a] Photonics Research Center, University of Malaya, 50603 Kuala Lumpur, Malaysia
[b] Department of Electrical Engineering, University of Malaya, 50603 Kuala Lumpur, Malaysia

ARTICLE INFO

Article history:
Received 21 February 2010
Received in revised form 18 May 2010
Accepted 18 May 2010
Available online 15 June 2010

Keywords:
Fiber optics displacement sensors
Concave mirror
Fiber optic sensors

ABSTRACT

Fiber optic displacement sensor (FODS) is proposed using a concave mirror for enhanced flexibility in sensitivity selection and linear range. The effect of focal length and diameter of the concave mirror on the displacement response is investigated. The experimental and theoretical results show that the second dip of the displacement response is located at distance equivalent to twice of focal length. For the third slopes and above, the sensitivity and the linear range of the sensor are strongly dependent on the focal length and diameter of the mirror. A good agreement between the theory and experimental results are shown. The measurement range as far as 26 mm can be achieved by using a 12 mm focal length concave mirror.

© 2010 Elsevier B.V. All rights reserved.

1. Introduction

Fiber optic displacement sensors (FODSs) are widely employed for the measurement of strain, pressure, vibration, temperature, etc., primarily due to their compactness, light weight, high sensitivity and immunity to a hostile environment. They can be classified into intensity-based and interferometry-based sensors [1,2]. For interferometry-based FODS, two optical waves with different optical paths are combined to generate interference fringes; one optical wave, the measurement wave is modulated by the displacement to be measured and the other optical wave, the reference wave, is not. The change in the displacement, therefore, alters the optical path difference between two waves resulting in a shift in the interference fringe pattern. As a result, the displacement change can be deduced from the measured fringe shift with ultra-high precision. However, this technique requires complicated instruments and is bandwidth limited. In comparison, an intensity-based FODS is simple to construct, uses less expensive components, and can have very high bandwidth [3].

Optical bundle fiber is typically used as a probe for intensity-based FODS. The amount of the light collected by the bundle fiber is directly correlated to the displacement between the fiber and the reflective surface. The geometry structure of the bundle fiber affects the transfer function and sensitivity of the FODS. The relationship between the blind region and peak position of the transfer function to the inclination angle and gap spacing between the transmitting core and receiving core have been intensively investigated and reported in many literatures [4,5]. On the other hand, some studies have shown that the type of reflective mirror in the configuration may have a crucial influence to the performance of the sensor. In the performance comparison between reflective mirrors with metallic and non-metallic surface, the metallic surface mirror has exhibited a greater sensitivity due to its spectacular reflection [6]. In this paper, a new intensity-based FODS is proposed and demonstrated using a bundle fiber as a probe and a concave reflective mirror as a target. A simulation model is presented and verified by an experimental measurement. The effect of focal length and diameter of the concave mirror on the performance of the FODS is also investigated. The proposed sensor has a longer dynamic range, which is very important in many applications such as in the meso-robotics field to undertake nano-positioning task on a wide stroke [7].

2. Theoretical simulation

The configuration of the proposed FODS which consists of a pair type bundle fiber and a concave mirror is shown in Fig. 1. As shown in the figure, the longitudinal axis of the transmitting fiber core is co-axis with the normal axis of concave mirror. The original laser source emitting point O is situated in the transmitting fiber and at a distance of z_a from the fiber surface end. After the reflection in the concave mirror, the reflected laser source is concentrated at point O′ and virtually becomes another emitting point source. Based on the spherical mirror equation, some important relations are determined as follows:

$$\frac{1}{u+z_a}+\frac{1}{v}=\frac{1}{f} \quad (1)$$

* Corresponding author at: Department of Electrical Engineering, University of Malaya, 50603 Kuala Lumpur, Malaysia.
E-mail address: swharun@um.edu.my (S.W. Harun).

0924-4247/$ – see front matter © 2010 Elsevier B.V. All rights reserved.
doi:10.1016/j.sna.2010.05.029

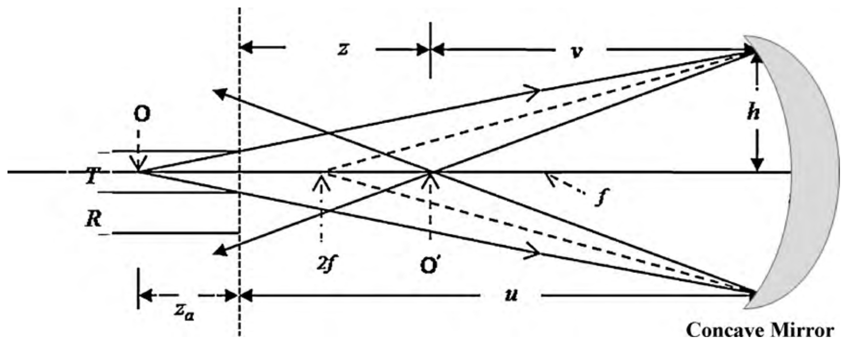

Fig. 1. Configuration of the proposed FODS.

where f denotes the focal length of the concave mirror while u is the distance between the sensor probe tip and concave mirror. v is the distance from the virtual point source to the concave mirror and is given by:

$$v = \frac{f(u+z_a)}{u-f+z_a} \quad (2)$$

Geometrically, the distance between the sensor probe tip and the virtual laser source can be determined by:

$$z = u - v$$

$$z = u - \frac{f(u+z_a)}{u-f+z_a} \quad (3)$$

The acceptance angle of the light cone from the virtual point source O′, θ' is given by:

$$\theta'(z) = \tan^{-1}\left(\left(\frac{u+z_a-f}{f}\right)\tan\theta\right) \quad (4)$$

where $\theta = \sin^{-1}$ (NA) and NA is the numerical aperture of the transmitting fiber.

The intensity of the light emitted from the transmitting core or fiber can be well described with Gaussian distribution [8] as shown in the following equation. The light intensity decays exponentially as it goes radially away from the center of the light circle:

$$I(r,z) = \frac{2P_E}{\pi\omega^2(z)} \exp\left(-\frac{2r^2}{\omega^2(z)}\right) \quad (5)$$

where r and z is the radial and longitudinal coordinate, respectively. $\omega(z)$ is the beam radius and expressed as a function of z as:

$$\omega(z) = \omega_0\sqrt{1+\left(\frac{z}{z_R}\right)^2} \quad (6)$$

The waist radius ω_0 and Rayleigh range z_R are the important parameters in the Gaussian Beam function and the detailed description can be found in Ref. [8]. For points situated in the far-field region, $z >> z_R$, the following relations with the acceptance angle can be obtained:

$$\theta \approx \tan\theta = \frac{\omega(z)}{z} = \frac{\omega_0}{z_R} = \frac{\lambda}{\pi\omega_0} \quad (7)$$

The beam radius of the virtual point source is $\omega(z) = z\theta'(z)$. The relation between the acceptance angle θ, transmitting fiber core radius r_t and z_a can be described by the equation below:

$$z_a = \frac{r_t}{\tan\theta} \quad (8)$$

By the approximation, $r_t = r_r = z_a \tan\theta \approx z_a\theta$. The radial distance from the core center of the transmitting fiber to the core center of receiving fiber is $r = 2z_a\theta$

Based on the properties above, the power harnessed by the receiving fiber, P can be evaluated by integrating the Gaussian distribution function (5) over the area of the receiving fiber end surface, S_r as:

$$P(r,z) = \int_{S_r} I(r,z)dS_r \quad (9)$$

where the core area of the receiving fiber is given by:

$$S_r = \pi r_r^2 = \pi z_a^2\theta^2 \quad (10)$$

Based on Eqs. (3), (4), (5) and (10), the received power as functions of displacement and focal length can be written as:

$$P(u,f) = \frac{2P_E}{\pi\omega^2(z)} \exp\left(-\frac{2r^2}{\omega^2(z)}\right) \times S_r = \frac{2P_E S_r}{(z\theta'(z))^2} \exp\left(-\frac{2(2z_a\theta)^2}{(z\theta'(z))^2}\right) \quad (11)$$

and therefore

$$P(u,f) = \frac{2z_a^2 P_E}{[u-((u+z_a)f/(u-f+z_a))]^2(((u+z_a)/f)-1)^2} \exp\left(-\frac{8z_a^2}{[u-(((u+z_a)f)/(u-f+z_a))]^2((u+z_a)/(f)-1))^2}\right) \quad (12)$$

In the near field sensing, most of the transmitted light from the bundled fiber is reflected back to bundled fiber as long as the incident light cone is within the reflecting surface area of the mirror. However, as the displacement increases the incident light cone grows larger. The maximum reflected light power from the mirror decreases due to the limited reflecting surface area of the mirror and subsequently influences the displacement response of the sensor. Thus, the reflecting surface area of the mirror becomes a significant parameter in the far-field analysis. The maximum reflected light power by the circular shape concave mirror is determined by:

$$E(D,u) = \int_0^{D/2} \frac{2}{\pi\omega^2(z)} \exp\left(-\frac{2r^2}{\omega^2(z)}\right) \cdot 2\pi r dr = \left[-\exp\left(-\frac{2r^2}{\omega^2(z)}\right)\right]_{r=0}^{D/2} \quad (13)$$

where D is the diameter of the concave mirror. Function $\omega(z)$ can be well approximated by $(u+z_a)\theta$, thus:

$$E(D,u) \approx 1 - \exp\left(-\frac{D^2}{2(u+z_a)^2\theta^2}\right) \quad (14)$$

In consideration of the limited reflecting surface area of the mirror, the displacement response of the proposed sensor is given

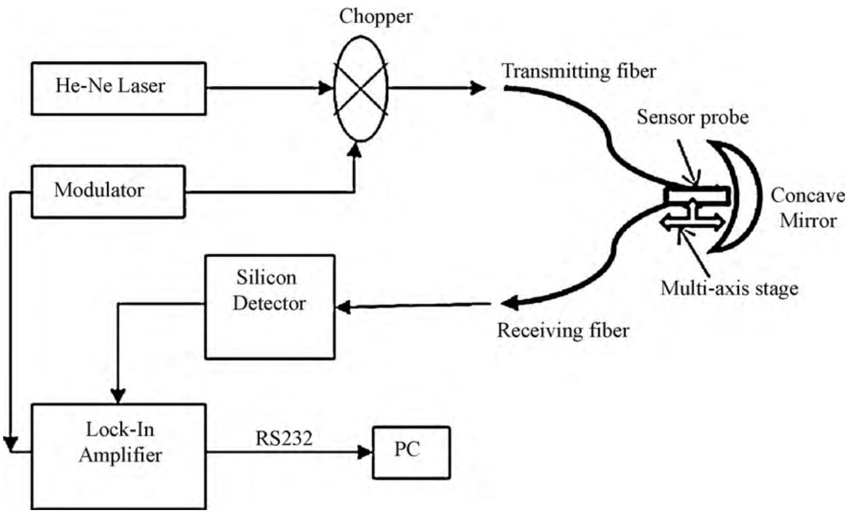

Fig. 2. Experimental set-up for the fiber optic displacement sensor with a concave mirror as the object.

by:

$$P_{rm}(u) = P(u,f) \times E(D,u) \quad (15)$$

which is governed by two important parameters, namely focal length f and the diameter of the circular concave mirror D.

3. Simulation and experiment

The theoretical model of the sensor is simulated using a MATLAB program. The theoretical results are then compared with the experimental one. Fig. 2 shows the experimental set-up used to test the sensor. The light from a He–Ne laser ($\lambda = 594$ nm) is coupled into a transmitting core and is emitted at the end of the bundle fiber to the concave mirror. The reflected light is then collected by the receiving core and transmitted to the silicon detector. The laser provides an average output power 3.0 mW, beam diameter 0.75 mm and beam divergence 0.92 mRads. The multimode plastic bundle fiber consists of two cores with a length of 2 m and core radius of 0.25 mm. The external chopper is used to modulate the laser at a frequency of 200 Hz before it is launched into the transmitting core. The concave mirror is fixed in a translation stage, which is controlled by a NewFocus Picomotor to multi-axial displacement. Displacement measurement is implemented in the y-axis direction while the other two axis's provide accurate alignment of the fiber probe and ensure that the longitudinal axis of the transmitting fiber is co-axis with the normal axis which is also located at the center of the concave mirror. Silicon detector measures the received light by the receiving fiber and converts it into electrical signal which is then denoised using the lock-in amplifier. The concave mirrors of four different focal lengths, 6 mm, 8 mm, 10 mm and 12 mm are used in this experiment and theoretical analysis. The effect of concave mirror diameter which represents the mirror aperture area is also investigated. Four different diameter values are used in the simulation and experiment; 12 mm, 16 mm, 20 mm and 24 mm for a fixed focal length of 10 mm.

4. Results and discussions

The basic principle of flat mirror based FODS can be found in the literature [4] and the essence of the following discussion focuses on the basic principle of concave mirror based FODS and its characteristic comparison with flat mirror FODS. Fig. 3 depicts two different displacement responses of FODS based on flat mirror and concave mirror. Due to two distinctive optical properties of the two mirrors,

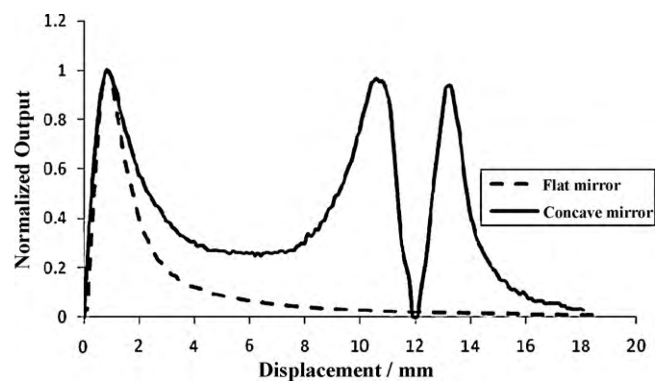

Fig. 3. The experimental results for displacement responses of flat mirror and concave mirror with $2f = 12$ mm.

two different characteristic curves are observed in the experiments. In the near displacement sensing range (0–4 mm), the displacement response of the proposed sensor shares the similar characteristic with the flat mirror FODS. As the sensor probe displaces further, the displacement response of the concave mirror FODS deviates from the displacement response of flat mirror FODS. Interestingly,

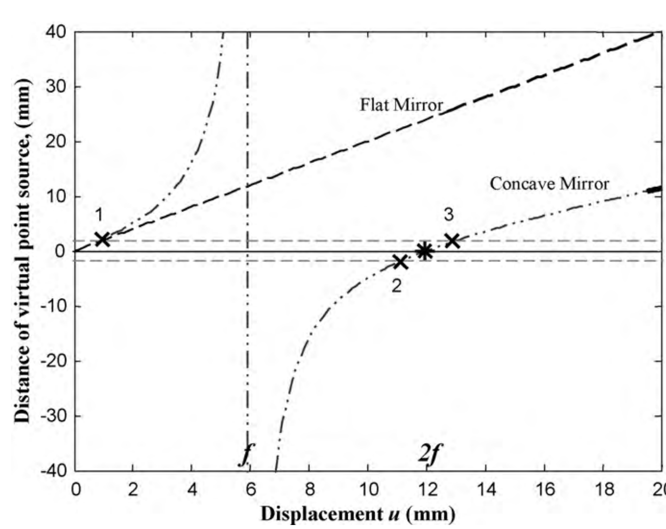

Fig. 4. Displacement of sensor probe against distance of virtual point source.

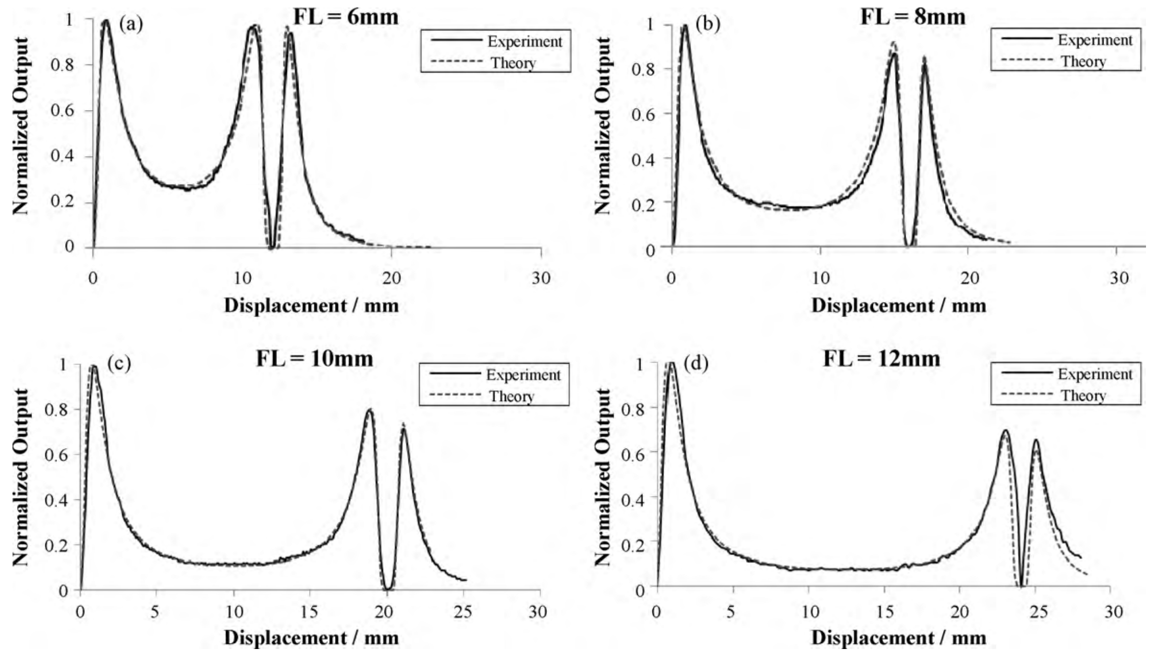

Fig. 5. The performance of the proposed FODS at various focal length (FL) (a) 6 mm, (b) 8 mm, (c) 10 mm and (d) 12 mm. The diameter of the concave mirror is fixed at 12 mm.

the displacement response reaches another two maximum points which are located sandwiching the point at *2f*. This can be explained by analyzing the location of the virtual point source in Fig. 4.

Fig. 4 depicts the relation between the displacement and virtual point source distance for two different configurations: flat mirror FODS and concave mirror FODS. The virtual point source distance is measured from sensor probe tip to virtual point source. In the near displacement range (0–4 mm), the flat mirror and concave mirror FODS shares the similar displacement variation and this explains the similarity of displacement responses between the two sensors in the range. As the sensor probe approaches the focal point ($u = f$) of the concave mirror, the location of the virtual point source is moving far away from the sensor probe thereby the displacement response comes to the first local minima. As the displacement u approaches *2f*, the displacement response reached the second local maxima and then the third local maxima which are marked by cross (×) symbols in Fig. 4. By observing all '×' marked points in Fig. 4, it is easy to find that three of virtual point sources are located at a specific distance from the sensor probe (approximately 2 mm). At $u = 2f$, the virtual point source is located at the end surface of the transmitting fiber (marked by '*') which light incident cone has become a small dot in the transmitting fiber

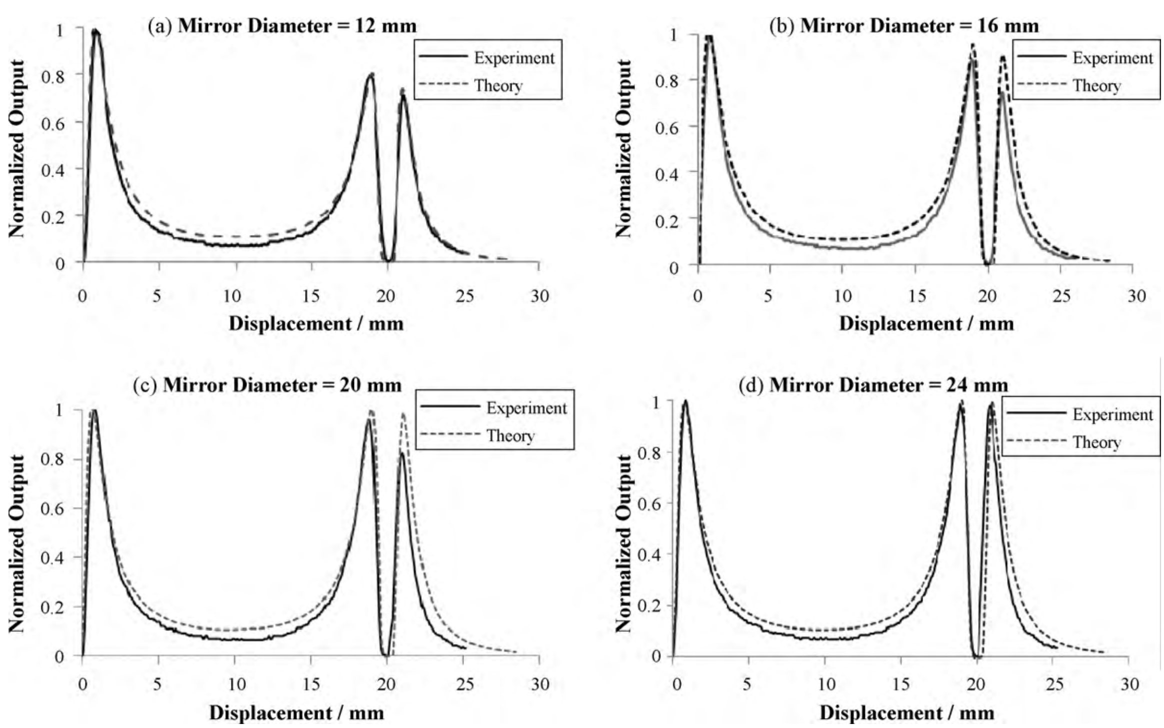

Fig. 6. The performance of the proposed FODS at various mirror diameters when the focal length is fixed at 10 mm. (a) 12 mm, (b) 16 mm, (c) 20 mm and (d) 24 mm.

core center and no light power can be collected by the receiving fiber.

Fig. 5 compares the theoretical and experimental displacement responses at various diameters of the concave mirror. As shown in the figure, the experimental curve is well agreed with the theoretical curve. There are six linear slopes in the displacement response and four of them are located in the vicinity of $u = 2f$ which is a function of the concave mirror focal length as depicted in the figure. This property enables flexible sensing based on displacement range of interest by properly choosing the desired focal length. In the observation, it is found that the received powers at second and third peaks of the displacement response decrease over the displacement as predicted in Eq. (14). As shown in Fig. 5(d), the measurement range as far as 26 mm is achieved by using a 12 mm focal length concave mirror. As the target is not flat, some portions of the experimental curves do not match with the theoretical curve as shown in Fig. 5. This is attributed to the probe end which is not exactly aligned to the concave center during experimental implementation.

Fig. 6(a)–(d) illustrates the influence of the mirror diameter (representation of mirror aperture area) to the displacement response of the proposed FODS. The larger is the mirror diameter, the nearer is the power of the second and third peaks to normalized power of 1. As shown in the figure, the first and second slopes of the FODS are not influenced by the mirror diameter. However, the third and the following slopes are strongly influenced by the mirror diameter. For instance, the linear range of the third slope can be improved by reducing the diameter. These results show that the proposed FODS offers a flexible sensing based on displacement range of interest by properly choosing the desired focal length and diameter of the mirror. In addition, the design for the proposed sensor is not restricted by the trade-off between linear range and sensitivity which is often encountered in the design of conventional flat mirror based FODS.

5. Conclusion

A concave mirror based FODS is proposed and demonstrated. A mathematical model is developed based on spherical properties of the concave mirror and the simulated results are found to be in good agreement with the experimental results. The study indicates that the focal length and the reflective aperture area of the mirror make significant influence to the displacement response curves. The displacement response curve has six slopes with the first two slopes show a similar characteristic with the conventional flat mirror based FODS. The other four slopes are located in the surrounding of $u = 2f$ which indicates the feasibility of selecting linear range of interest based on the concave mirror focal length and diameter. The measurement range as far as 26 mm can be achieved by using a 12 mm focal length concave mirror.

References

[1] P.K. Rastogi, Optical Measurement Techniques and Applications, Artech House, Inc., Boston, London, 1997.
[2] D.W. Kim, Y. Zhang, K.L. Cooper, A. Wang, In-fiber reflection mode interferometer based on a long-period grating for external refractive-index measurement, Applied Optics 44 (26) (2005) 5368–5373.
[3] P.B. Buchade, A.D. Shaligram, Simulation and experimental studies of inclined two fiber displacement sensor, Sensor and Actuators A 128 (2006) 312–316.
[4] S.W. Harun, H.Z. Yang, M. Yasin, H. Ahmad, Theoretical and experimental study on the fiber optic displacement sensor with two receiving fibers, Microwave and Optic Technology Letters 52 (2009) 373–375.
[5] H.Z. Yang, S.W. Harun, H. Ahmad, Fiber optic displacement and liquid refractive index sensors with two asymmetrical inclined fibers, Sensor and Transducer 108 (2009) 80–88.
[6] K.S. Lim, S.W. Harun, H.Z. Yang, K. Dimyati, H. Ahmad, Analytical and experimental studies on asymmetric bundle fiber displacement sensors, Journal of Modern Optics 56 (2009) 1838–1842.
[7] C. Prelle, F. Lamarque, P. Revel, Reflective optical sensor for long-range and high resolution displacements, Sensor and Actuators A 127 (2006) 139–146.
[8] H.M. Cao, Y.P. Chen, Z.D. Zhou, G. Zhang, Theoretical and experimental study on the optical fiber bundle displacement sensors, Sensor and Actuators A 136 (2007) 580–587.

Biographies

Yang Hang Zhou was born in Xi'an City, China, on September 22, 1981. He received the B.S. degree in telecommunication engineering from Air Force Engineering University, China in 2005, and the M.Eng in telecommunication engineering from University of Malaya, Malaysia in 2009. He is currently working towards the Ph.D. degree at University of Malaya. His current research interest is in fiber optic sensor.

Lim Kok Sing obtained his B.Eng degree from University of Malaya in 2008. Currently, he is pursuing his Ph.D. in fiber optic technology at Physics Department, University of Malaya, Malaysia.

Sulaiman Wadi Harun received the B.E. degree in electrical and electronics system engineering from Nagaoka University of Technology, Japan in 1996, and M.Sc. and Ph.D. degrees in physics from University of Malaya in 2001 and 2004, respectively. Currently, he is an associate professor at the Faculty of Engineering, University of Malaya. His research interests include fiber optic active and passive devices.

Kaharudin Dimyati obtained his Ph.D. from the University of Wales Swansea (U.K.) in 1996. He is a professor in Department of Electrical Engineering, University of Malaya.

Harith Ahmad received the Ph.D. degree in laser technology from the University of Wales Swansea (U.K.) in 1983. He is a professor at the Department of Physics, University of Malaya. He is also a fellow member of Malaysian Academic of Science.

This article was downloaded by: *[Hong Kong University of Science & Tech]*
On: *4 January 2011*
Access details: *Access Details: [subscription number 907916909]*
Publisher *Taylor & Francis*
Informa Ltd Registered in England and Wales Registered Number: 1072954 Registered office: Mortimer House, 37-41 Mortimer Street, London W1T 3JH, UK

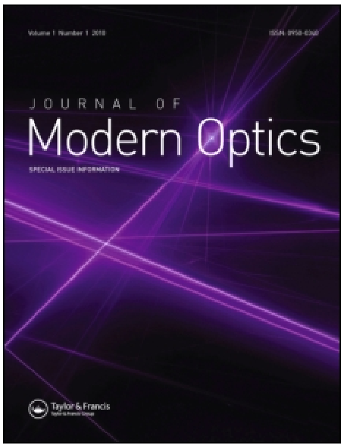

Journal of Modern Optics
Publication details, including instructions for authors and subscription information:
http://www.informaworld.com/smpp/title~content=t713191304

Analytical and experimental studies on asymmetric bundle fiber displacement sensors

K. S. Lim[a]; S. W. Harun[ab]; H. Z. Yang[a]; K. Dimyati[b]; H. Ahmad[a]
[a] Department of Physics, Faculty of Science, University of Malaya, Kuala Lumpur, Malaysia [b] Department of Electrical Engineering, Faculty of Engineering, University of Malaya, Kuala Lumpur, Malaysia

First published on: 26 October 2009

To cite this Article Lim, K. S. , Harun, S. W. , Yang, H. Z. , Dimyati, K. and Ahmad, H.(2009) 'Analytical and experimental studies on asymmetric bundle fiber displacement sensors', Journal of Modern Optics, 56: 17, 1838 — 1842, First published on: 26 October 2009 (iFirst)

To link to this Article: DOI: 10.1080/09500340903366009
URL: http://dx.doi.org/10.1080/09500340903366009

PLEASE SCROLL DOWN FOR ARTICLE

Full terms and conditions of use: http://www.informaworld.com/terms-and-conditions-of-access.pdf

This article may be used for research, teaching and private study purposes. Any substantial or systematic reproduction, re-distribution, re-selling, loan or sub-licensing, systematic supply or distribution in any form to anyone is expressly forbidden.

The publisher does not give any warranty express or implied or make any representation that the contents will be complete or accurate or up to date. The accuracy of any instructions, formulae and drug doses should be independently verified with primary sources. The publisher shall not be liable for any loss, actions, claims, proceedings, demand or costs or damages whatsoever or howsoever caused arising directly or indirectly in connection with or arising out of the use of this material.

Journal of Modern Optics
Vol. 56, No. 17, 10 October 2009, 1838–1842

Taylor & Francis
Taylor & Francis Group

Downloaded By: [Hong Kong University of Science & Tech] At: 04:46 4 January 2011

Analytical and experimental studies on asymmetric bundle fiber displacement sensors

K.S. Lim[a], S.W. Harun[a,b]*, H.Z. Yang[a], K. Dimyati[b] and H. Ahmad[a]

[a]*Department of Physics, Faculty of Science, University of Malaya, Lembah Pantai 50603, Kuala Lumpur, Malaysia;* [b]*Department of Electrical Engineering, Faculty of Engineering, University of Malaya, Lembah Pantai 50603, Kuala Lumpur, Malaysia*

(*Received 30 June 2009; final version received 24 September 2009*)

A fiber-optic displacement sensor (FODS) is theoretically and experimentally studied using an asymmetrical bundled fiber. The bundled fiber consists of two parallel fibers with different core radial ratios (CRRs) to achieve different sensitivity and dynamic range for displacement measurements. Both analytical modeling and experimental observations show that the linear range and sensitivity can be adjusted by controlling the CRR between transmitting and receiving fibers. This increases the flexibility of the sensor, which can be used for precise non-contact sensing applications.

Keywords: fiber-optic displacement sensor; bundled multimode fiber; asymmetric bundle fiber sensor

1. Introduction

Multimode plastic fiber plays an important role for the transmission and processing of the optical signal in communication and sensor applications. This fiber has a large core size with a relatively high numerical aperture, which is suitable for the signal coupling and receiving of reflected light from a target in sensor applications [1,2]. Based on the merits mentioned, multimode plastic fiber is found to be perfectly suited for optical displacement sensing applications. For this application, a two-fiber probe is normally used in conjunction with an intensity modulation technique. This type of sensor provides a promising solution for displacement measurement in terms of a wide dynamic range, with high potential for ultra-precise non-contact sensing. It also provides flexibility for incorporating the optical sensors permanently into composite structures for monitoring purposes [3].

In most of the fiber-optical displacement sensors [4–12], the radii of the transmitting and receiving fibers are often made the same for the convenience of analytical study and experiments. However, there is a lack of research work on displacement sensors using bundled fibers with different core radii. In this paper, a mathematical model of a displacement sensor using asymmetrical bundled fibers is developed. Some simulations were carried out based on the mathematical model and experimental results were also obtained to validate the MATLAB simulated results. The effects of different core radial ratios (CRRs) on the dynamic range, sensitivity and illumination area of bundled fibers are analyzed and discussed.

2. Modeling of the asymmetric bundle fiber displacement sensor

The proposed fiber-optic displacement sensor (FODS) consists of transmitting and receiving fibers as well as a reflecting mirror. Both fibers are of different core radius and are bundled together in parallel, as shown in Figure 1. Let r_T and r_R denote the core radius of the transmitting fiber and the core radius of the receiving fiber. The core radial ratio, CRR is the ratio of the transmitting fiber core radius and the receiving fiber core radius, as given below:

$$\text{CRR},\quad k = \frac{r_R}{r_T}. \tag{1}$$

Figure 2 shows the geometric illustration of the overlapping area between the reflected light circle and the core of the receiving fiber at different CRRs. Based on this figure, with the same core radius of the transmitting fiber; the reflected light power collected by the receiving fiber increases with the increasing core radius of the receiving fiber. The larger the receiving fiber core radius and core area, the larger fraction of reflected light can be collected by the receiving fiber. In a previous report [10], two major approaches were introduced for theoretical analysis, namely the geometrical and Gaussian beam approaches. For the

*Corresponding author. Email: swharun@um.edu.my

ISSN 0950–0340 print/ISSN 1362–3044 online
© 2009 Taylor & Francis
DOI: 10.1080/09500340903366009
http://www.informaworld.com

Downloaded By: [Hong Kong University of Science & Tech] At: 04:46 4 January 2011

former, the simple assumption is made that the light intensity is constant within the reflected light circle. On the other hand, the light intensity outside the reflected light circle is null. This approach is apparently less accurate compared with the second approach. The Gaussian beam approach is a more realistic and more accurate method. The intensity of the light emitted from the transmitting fiber is described with a Gaussian distribution, as shown in Equation (2). The light intensity decays exponentially as it moves radially away from the center of the light circle.

$$I(r,z) = \frac{2P_E}{\pi\omega^2(z)} \exp\left(-\frac{2r^2}{\omega^2(z)}\right) \tag{2}$$

where r is the radial coordinate, z is the longitudinal coordinate from the light origin. $\omega(z)$ is the beam radius which is also a function of z, and

$$\omega(z) = \omega_0 \sqrt{1 + \left(\frac{z}{z_R}\right)^2}.$$

The waist radius ω_0 and Rayleigh range z_R are the important parameters in the Gaussian beam function.

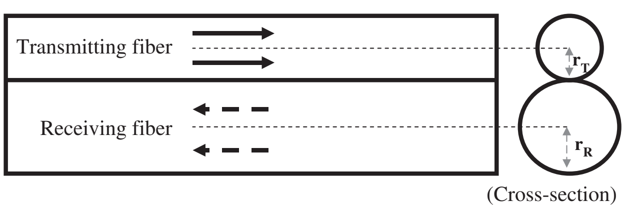

Figure 1. Side and front views of the transmitting and receiving fiber ends.

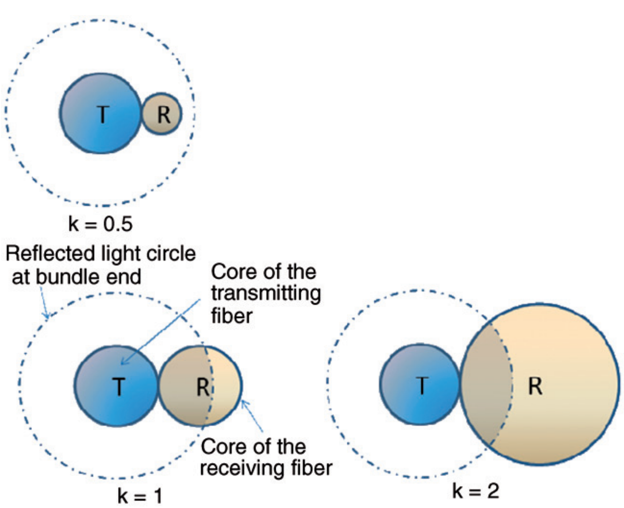

Figure 2. Geometrical illustration for the overlapping area between the reflected light circle and the core of the receiving fiber at different CRRs. T and R are the transmitting and receiving fibers, respectively. (The color version of this figure is included in the online version of the journal.)

The light power collected by the receiving fiber can be evaluated by using the integral as shown in Equation (3).

$$P(z) = \int_{S_R} I(r,z)\,\mathrm{d}S_R. \tag{3}$$

However, the exact integration is tedious and impossible. Therefore, assumptions and approximations were used to solve the integration. For points situated in the far-field, $z \gg z_R$ the following relations with the divergence angle can be obtained

$$\theta_a = \tan\theta_a = \frac{\omega(z)}{z} = \frac{\omega_0}{z_R} = \frac{\lambda}{\pi\omega_0}. \tag{4}$$

The core radius of the transmitting fiber and receiving fibers are given by the approximation

$$r_T = z_a \tan\theta_a \approx z_a\theta_a \tag{5}$$

and

$$r_R = k\omega_T = kz_a\theta_a \tag{6}$$

where z_a is the distance between the beam source to the fiber end [10]. The core area of the receiving fiber is computed from

$$S_a = \pi r_R^2 = \pi k^2 z_a^2 \theta_a^2. \tag{7}$$

The radial distance between the two core centers of the transmitting fiber and receiving fiber is determined from

$$r = r_T + r_R = r_T + kr_T = (1+k)z_a\theta_a. \tag{8}$$

The path of the beam from the beam source to the bundle end after the reflection is given by

$$z_a + 2h. \tag{9}$$

The displacement parameter in the normalized form is presented as

$$\zeta = \frac{z_a + 2h}{z_a} \tag{10}$$

or

$$\zeta = 1 + 2h_N \tag{11}$$

where $h_N = h/z_a$. To relate the displacement between the reflective mirror to the fiber end, h, to the transfer function, with the help of the results determined above, the collected power of the receiving fiber can be expressed as

$$\begin{aligned} P(h) &= \frac{2P_E}{\pi\omega^2(z_a+2h)} \exp\left(-\frac{2r^2}{\omega^2(z_a+2h)}\right) \times S_a \\ &= \frac{2P_E k^2 z_a^2}{(z_a+2h)^2} \exp\left(-\frac{2((1+k)z_a)^2}{(z_a+2h)^2}\right). \end{aligned} \tag{12}$$

Downloaded By: [Hong Kong University of Science & Tech] At: 04:46 4 January 2011

By substituting Equation (10) into this equation, we obtain

$$P(\xi) = \frac{2P_E k^2}{\xi^2}\exp\left(-\frac{2(1+k)^2}{\xi^2}\right). \quad (13)$$

The maximum received power is achieved when $P'(\xi) = 0$, and this leads to

$$\xi_{\max} = \sqrt{2}(1+k). \quad (14)$$

Based on the above equations, the maximum h is given by

$$h_{\max} = \frac{\sqrt{2}k + \sqrt{2} - 1}{2}. \quad (15)$$

The maximum power is given by

$$P_{\max} = P(\sqrt{2}(1+k)) = \frac{k^2 P_E}{(k+1)^2}\exp(-1). \quad (16)$$

In the normalized form, Equation (10) is rewritten as

$$P_N(\xi) = \frac{P(\xi)}{P_{\max}} = \frac{2(k+1)^2}{\xi^2}\exp\left(1 - \frac{2(1+k)^2}{\xi^2}\right). \quad (17)$$

In the analysis, the theoretical model of the FOD sensor is modeled based on the similar parameters used in the experiment: the wavelength of the laser source $\lambda = 594$ nm, the transmitting fiber core radius $r_R = 0.5$ mm and numerical aperture value NA = 0.4. Based on the same parameters, four analytical models were simulated for $k = 0.5$, 1, 2 and 3, which were based on the available fiber core radius combinations in the experiments.

3. Experiment

Figure 3 shows the experimental set-up for the FODS using the bundled fiber with different core radii. The asymmetrical bundled fiber is constructed by pairing two different plastic fibers with the core radii of either 0.25 mm or 0.50 mm or 0.75 mm. Owing to the limited selections of core diameters, six combinations were selected for the experiments: $[k, r_T, r_R] = [0.5, 0.5\text{ mm}, 0.25\text{ mm}]$, [1.0, 0.5 mm, 0.5 mm], [2.0, 0.25 mm, 0.5 mm] and [3.0, 0.25 mm, 0.75 mm]. k is the core radial ratio. The light source is emitted from a source of 594 nm wavelength, yellow HeNe laser and modulated using a chopper spinning at a frequency of 200 Hz. The modulated light beam is then launched into one of the fibers in 2 m long bundled plastic fiber – the transmitting fiber. The fiber probe is placed perpendicularly to the reflecting mirror.

The light beam emitted from the transmitting fiber is reflected by the flat mirror and the receiving fiber collects the reflected light. A precise displacement reference between the bundle end and the reflecting mirror is imperative for the experiment. Therefore, a New Focus 9061 motorized stage, driven by a picomotor, is used to change the displacement of the reflecting mirror from the fiber probe. Each incremental step in the displacement is made identical and accurate. The collected light power in the receiving fiber is converted by a silicon detector into electrical power. Lastly, the electrical signal is filtered by a lock-in amplifier and recorded in the computer.

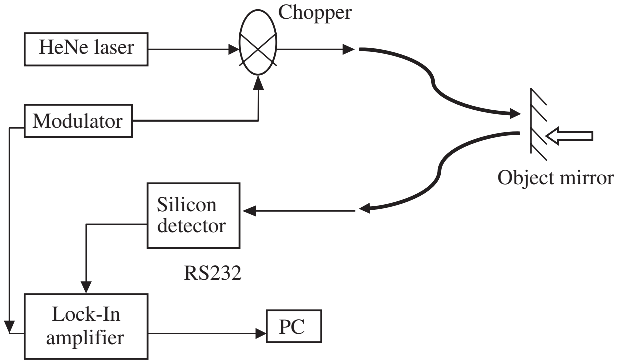

Figure 3. Experiment set-up.

4. Results and discussion

In both the theoretical and experimental analysis, the results are processed and displayed in the normalized forms in which the output power is normalized by the maximum output power and the displacement is normalized by the parameter z_a. This makes the output function a dimensionless function and eliminates the dependency of the FODS output function on the fiber core radius and divergence angle. Figures 4 and 5 show the analytical and experimental results,

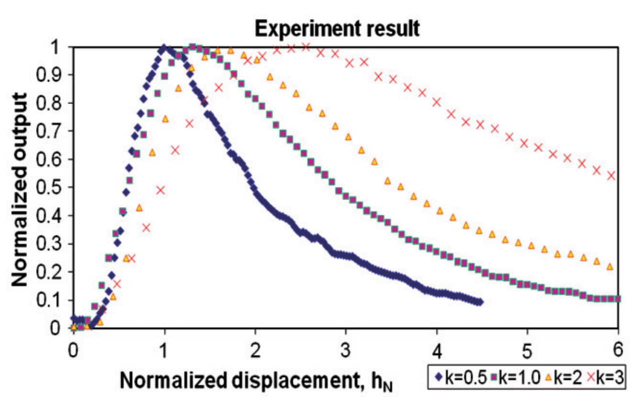

Figure 4. The experimental result of proposed FODS model at different CRRs or k values. (The color version of this figure is included in the online version of the journal.)

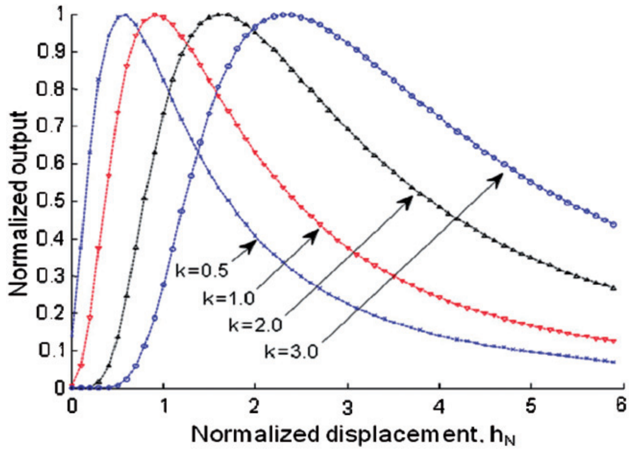

Figure 5. The theoretical result of the fiber displacement sensor at different CRRs or k values. (The color version of this figure is included in the online version of the journal.)

respectively, for the proposed FODS. As shown in both figures, the location of the maximum output is shifted toward the right along the axis of displacement as the value of k increases. In addition, the linear range on the front slope and back slope gets larger for every larger value of k. Both graphs exhibit almost the same characteristics in the curves as the value of k increases. This phenomenon can be explained by the use of the distinctive core radius of the two fibers. As shown in Figure 2, for the same displacement, the fraction of the overlap area in the receiving fiber core by the reflected light circle (shaded area percentage in the receiving fiber core) differs for different CRR. For a larger value of k, the fiber displacement sensor requires further displacement to achieve the maximum overlap area. Adversely, the sensitivity of the fiber displacement sensor decreases as the CRR increases. On the other hand, some error in the initial displacement ($0 < h < 0.3$) is observed if the two overlaid graphs are compared. This error accounts for the approximation used in the theoretical analysis.

The performance of the proposed FODS from the experimental results is summarized in Table 1. The results show that the magnitude of the sensitivity decreases as the CRR or k value becomes larger while the linear range is larger for a larger value of k. The sensitivity characteristic trend is consistent with the theoretical plot, as shown in Figure 6. Figure 6 shows the normalized sensitivity against normalized displacement at various k values. The curve width of the graph represents the linear range of the sensor. As shown in the figure, the linear range of the sensor increases with the value of k which is in agreement with the experimental result in Table 1. This property provides a greater enhancement in FODS applications in terms of flexibility, wider dynamic range and high precision

Table 1. The sensitivity and linear range for different k values.

CRR, k	Front slope sensitivity	Linear range	Back slope sensitivity	Linear range
0.5	1.7615	0.320–0.800	−0.5270	1.312–1.176
1	1.0984	0.230–0.998	−0.3378	1.536–3.302
2	0.9688	0.288–1.296	−0.2581	1.728–4.320
3	0.6955	0.320–1.440	−0.1366	2.240–5.400

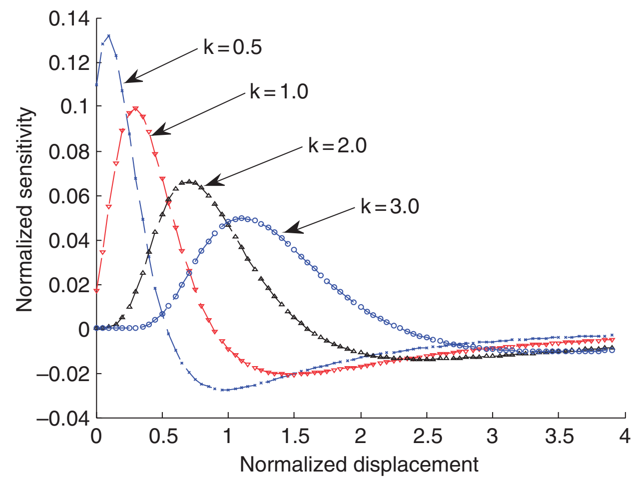

Figure 6. Theoretical normalized sensitivity curves of the fiber displacement sensor at various k values. (The color version of this figure is included in the online version of the journal.)

displacement measurement. The maximum sensitivity of 1.76 is obtained at $k = 0.5$. The largest dynamic range of 3.16 is obtained at $k = 3$. The conventional FODS, which uses two fibers with identical core radii, often encounters several restrictions owing to the limited linear range for the measurement. In addition, the limited sensitivity option often becomes a challenge in high-precision measurement. This restriction can be avoided using a suitable CRR or k value. The k value can be chosen in a way to provide the optimum performance.

5. Conclusion

The performance of FODS with asymmetrical bundled fiber is theoretically and experimentally demonstrated. The effect of different core radial ratios (CRRs) on the performance of the sensor is investigated in terms of dynamic range and sensitivity. The experimental results are almost in agreement with the theoretical results. The location of the maximum output is shifted toward the right along the axis of displacement as the value

Downloaded By: [Hong Kong University of Science & Tech] At: 04:46 4 January 2011

of *k* increases. In addition, the linear range for both front and back slopes increases with the value of *k*.

References

[1] Nalwa, S. *Polymer Optical Fibres*; American Scientific Publishers: California, 2004.
[2] Kulkarini, V.K.; Lalasangi, A.S.; Pattanashetti, I.I.; Raikar, U.S. *J. Optoelectron. Adv. Mat.* **2006,** *8,* 1610–1612.
[3] Spooncer, R.C.; Butler, C.; Jones, B.E. *Opt. Eng.* **1992,** *31,* 1632–1637.
[4] Murphy, M.M.; Jones, G.R. *Pure Appl. Opt.* **1994,** *3,* 361–369.
[5] Wang, D.-X.; Karim, M.A.; Li, Y. *Opt. Eng.* **1997,** *36,* 838–842.
[6] Ko, W.H.; Chang, K.-M.; Hwang, G.-J. *Sensor Actuat. A – Phys.* **1995,** *49,* 51–55.
[7] Bock, W.J.; Nawrocka, M.S.; Urbanczyk, W. *IEEE Trans. Instrum. Meas.* **2001,** *50,* 1085–1088.
[8] Elasar, J.; Selmic, S.; Tomic, M.; Prokin, M. *J. Opt. A: Pure Appl. Opt.* **2002,** *4,* 347–355.
[9] Oiwa, T.; Nishitani, H. *Meas. Sci. Technol.* **2004,** *15,* 84–90.
[10] Faria, J.B. *IEEE T. Instrum. Meas.* **1998,** *47,* 742–747.
[11] Cao, H.; Chen, Y.; Zhou, Z.; Zhang, G. *Sensor Actuat A – Phys.* **2007,** *136,* 580–587.
[12] Buchade, P.B.; Shaligram, A.D. *Sensor Actuat. A – Phys.* **2006,** *128,* 312–316.

Downloaded By: [Hong Kong University of Science & Tech] At: 04:46 4 January 2011

Theoretical and experimental studies on liquid refractive index sensor based on bundle fiber

S.W. Harun
Department of Electrical Engineering, University of Malaya, Kuala Lumpur, Malaysia, and

H.Z. Yang and H. Ahmad
Physics Department, University of Malaya, Kuala Lumpur, Malaysia

Abstract

Purpose – The purpose of this paper is to investigate, theoretically and experimentally the performance of liquid refractive index sensor (LRIS).
Design/methodology/approach – The proposed LRIS is based on the intensity modulation and a bundle fiber. The mathematical model is used to study the effect of inclination angle on performance of the sensor.
Findings – The theoretical result shows that the highest sensitivity can be achieved by using a probe inclined with angle 20° which is almost 13 times higher than that of 0° inclination. In the experiment, three different liquids: isopropyl alcohol, water and methanol are used to investigate the sensor response. Both theoretical and experimental results show that the peak power and the location of the displacement curve changes with refractive index. The sensitivities are obtained at 0.11/mm and 0.04/mm for the sensors with 10° and 0° inclination angles, respectively.
Originality/value – In this paper, a simple LRIS is proposed using a bundle fiber as a probe at various inclination angles.

Keywords Fiber optic sensors, Refraction

Paper type Research paper

1. Introduction

Fiber-optic displacement sensors (FODSs) have been intensively studied and experimented due to their many desirable advantages such as small size, high sensitivity, immunity of electromagnetic interference and safety for hazardous or explosive environment (Rastogi, 1997). This sensor consists of two pieces of fibers, one set connected to a light source and termed the transmitting fiber, and the other set connected to a photo detector (photodiode) and known as the receiving fiber. Both fibers are bundled into a common probe. The FODS has the capability to measure physical quantities such as the displacement, vibration, strain, pressure, etc. (Lim *et al.*, 2009; Yasin *et al.*, 2009, 2007; Suhadolnik *et al.*, 1995). However, the use of this sensor for detection of environmental refractive index change has not been fully explored. Refractive index sensor is important for biological and chemical applications since a number of substances can be detected through measurements of the refractive index. For the liquid refractive index sensor (LRIS), an intensity modulation is normally used in conjunction with multimode plastic fiber because of its many advantages such as non-contact sensing. The use of the multimode plastic fiber provides an efficient signal coupling as well as being able to receive the maximum reflected light from a target (Nath *et al.*, 2008).

A FODS-based refractive index measurement using a bundle fiber was first introduced by Suhadolnik *et al.* (1995). Later on Chaudhari and Shaligram (2002) reported on the study of LRIS at various types of optical sources. In our earlier work, a FODS was proposed based on two asymmetrical fibers for liquid refractive index measurement (Yang *et al.*, 2009). In this paper, a new LRIS is proposed and demonstrated using a pair type of bundle at various inclination angles. A mathematical model is developed to investigate the performance of the sensor with different inclination angles. An experiment is also carried out to investigate the sensor performance at various liquid materials.

2. Mathematical model

The structure of the proposed LRIS is shown in Figure 1, which consists of a pair of transmitting and receiving fibers. We assume that the transmitting and receiving fibers have inclination angles of θ_1 and θ_2, respectively, against the y-axis. To evaluate the amount of light illuminating the receiving fiber, the light cone from the image of the transmitting which is located opposite of the mirror with the same distance, is analyzed. The central of the receiving fiber and the image of transmitting fiber are denoted as O' and O, respectively. As shown in Figure 1, the light leaving the transmitting fiber is represented by a perfectly symmetrical cone with divergence angle α and vertex O located at a distance z_a inside the fiber.

From the geometrical analysis of Figure 1, $\alpha = \sin^{-1}(NA/n)$, and $z_a = r_1/tan\alpha$. Therefore, the following distances are given by:

The current issue and full text archive of this journal is available at **www.emeraldinsight.com/0260-2288.htm**

Sensor Review
31/2 (2011) 173–177
© Emerald Group Publishing Limited [ISSN 0260-2288]
[DOI 10.1108/02602281111110031]

Figure 1 Structure of sensor probe

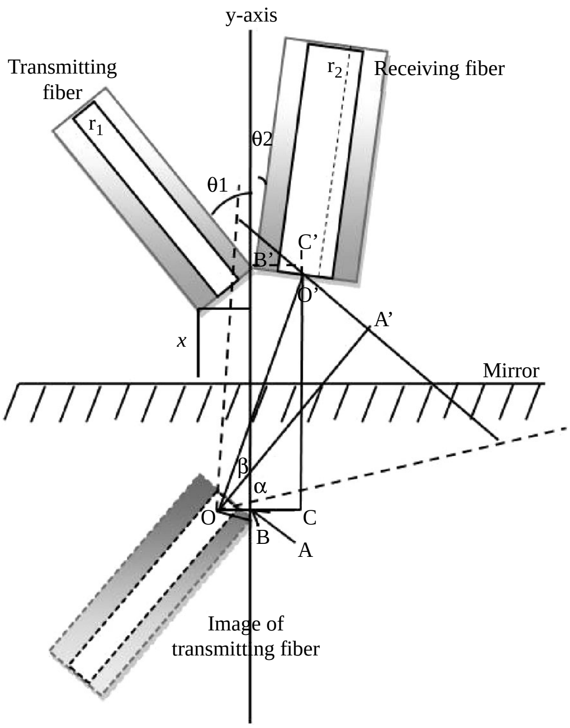

$$AB = \sqrt{z_a^2 + r_{d1}^2}\sin\left(\tan^{-1}\left(\frac{r_{d1}}{z_a}\right) - \frac{\pi}{2} + \theta_1\right) \quad (1)$$

$$O'C = 4r_{d1}\sin\theta_1 + 2x - AB - r_{d2}\sin\theta_2 \quad (2)$$

$$OA = \sqrt{z_a^2 + r_{d1}^2}\cos\left(\tan^{-1}\left(\frac{r_{d1}}{z_a}\right) - \frac{\pi}{2} + \theta_1\right) \quad (3)$$

$$OC = OA + r_{d2}\cos\theta_2 \quad (4)$$

$$OO' = \sqrt{O'C^2 + OC^2} \quad (5)$$

where the NA is numerical aperture of transmitting fiber, n is refractive index of liquid, r_1 and r_2 are the core radius of transmitting fiber and receiving fiber while the r_{d1} and r_{d2} are the radius of transmitting fiber and receiving fiber, respectively, and the x is the displacement between the sensor probe tip and reflector mirror.

Also from the geometrical analysis, the acceptance angle β of the light cone from the virtual point source O, is given by:

$$\beta(z) = \tan^{-1}\left(\frac{O'C}{OC}\right) - \frac{\pi}{2} + \theta_1 \quad (6)$$

The intensity of the light emitted from the transmitting fiber can be well described with Gaussian distribution (Lim *et al.*, 2009) and is given by:

$$I(r,z) = \frac{2P_E}{\pi\omega^2(z)}\exp\left(-\frac{2r^2}{\omega^2(z)}\right) \quad (7)$$

where P_E is the emitted power from the light source, r is the radial coordinate and z is the longitudinal coordinate. $\omega(z)$ is the beam radius and expressed as a function of z, $\omega(z) = \omega_0\sqrt{1 + (z/z_R)^2}$. The waist radius ω_0 and Rayleigh range z_R are the important parameters in the Gaussian beam function and the detailed description can be found in Lim *et al.* (2009). Equation (7) shows that the light intensity decays exponentially as it goes radially away from the center of the light circle. The radial coordinate r of equation (7) can be determined by:

$$r = OO'\sin\beta \quad (8)$$

The longitudinal coordinate is the distance between the sensor probe tip and the virtual laser source point O and it can be determined:

$$z = OO'\cos\beta \quad (9)$$

For points situated in the far field $z \gg z_R$, the beam radius of the virtual point source can be derived as (Kleiza and Verkelis, 2007):

$$\omega(z) \approx z\alpha \quad (10)$$

By the approximation:

$$r_1 = z_a\tan\alpha \approx z_a\alpha \quad (11)$$

Based on the properties above, the power harnessed by the receiving fiber, P can be evaluated by integrating the Gaussian distribution function of equation (7) over the area of the of receiving fiber end surface, S_r:

$$P(r,z) = \int_{S_r} I(r,z)dS_r \quad (12)$$

where the core area of the receiving fiber is:

$$S_r = \pi r_1^2 = \pi z_a^2\alpha^2 \quad (13)$$

By combining and substituting equations (8), (9), (10) and (13) into the equation (12), finally the proposed LRIS response can be summarized as:

$$P_{(z,r)} = \frac{2P_E}{\pi\omega^2(z)}\exp\left(-\frac{2r^2}{\omega^2(z)}\right) \times S_r = \frac{2z_a^2P_E}{z^2}\exp\left(\frac{2r^2}{z^2\alpha^2}\right) \quad (14)$$

This equation shows that the liquid refractive index response of sensor is a function of displacement x and refractive index n of surrounding medium while sensor probe is design of inclination angles of θ_1 and θ_2. Therefore, based on equation (14), the proposed LRIS can be used to detect the liquid refractive index where the sensor probe is immersed by the measurement liquid. Table I shows the list of all variables used in this section and its definition.

3. Simulation and experiment

The mathematical model of the proposed LRIS is simulated by MATLAB programming. In the simulation, the wavelength of the laser source λ and numerical aperture NA is set at 594 nm and 0.32, respectively. The fiber core radius r_1 and r_2 are set at 0.25 and 0.5 mm while the fiber diameters r_{d1} and r_{d2} are set at 0.5 and 0.75 mm, respectively. Figure 2 shows the experimental setup, which consists of a 594 nm yellow He-Ne laser source and a bundled fiber probe. The emitted light source has

Sensor Review
Volume 31 · Number 2 · 2011 · 173–177

Table I List of all variables

Variables	Definitions
NA	The numerical aperture of transmitting fiber
n	The refractive index of liquid
r_1	Core radius of transmitting fiber
r_2	Core radius of receiving fiber
r_{d1}	Radius of transmitting fiber
r_{d2}	Radius of receiving fiber
x	The displacement moving of sensor probe and mirror
P_E	The output power of laser source
r	The radial coordinate
z	The distance between the sensor probe tip and the virtual laser source point

Figure 2 Experimental setup of the proposed LRIS

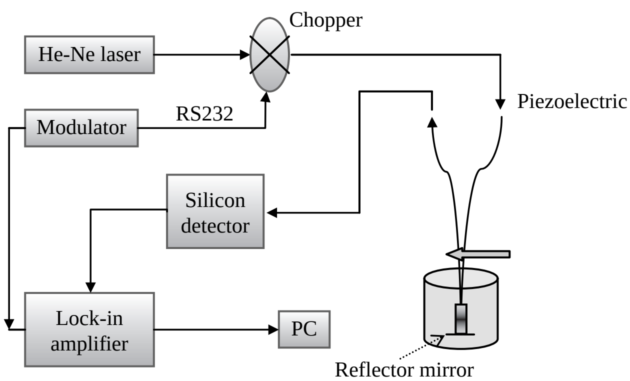

an average output power of 3.0 mW, beam diameter of 0.75 mm and beam divergence 0.92 of mRads. The external chopper is used to modulate the light at a frequency of 200 Hz before it is launched into the transmitting fiber. The transmitting fiber transfers the modulated light to a reflective mirror while the receiving fiber collects the reflected light, which is then transferred to the detector. The sensor probe is mounted on the stage controlled by NewFocus Picomotor for the displacement measurement. Silicon detector is used to measure the received light and converts it into electrical signal which is then denoised using a lock-in amplifier. During the measurement, the room temperature is maintained at 28°C to avoid the change of liquid refractive index.

4. Results and discussions

Figure 3 shows the sensor responses at different probe inclination angles θ_1 and θ_2 for three different refractive indices of 1, 1.3 and 1.6. In the simulation, the probe is inclined with the same angles of 0°, 10° and 20°, the outputs powers are normalized into 1 and unit of the displacement is mm. Figure 3 shows three different sensor responses, which were group based on the three different inclination angles. As seen in Figure 3, it was found that the inclination angles θ_1 and θ_2 reasonably affect the displacement curves profile and output power. The highest output power is almost ten times of the lowest output power. The vertical dash lines are located in the displacements of 1.1, 2.0 and 3.4 mm corresponding to the sensor probe inclination angles of 20°, 10° and 0°, respectively. Comparing those positions, the sensor responses have the biggest output power differentiation when the refractive index is increased from 1.0 to 1.6. The sensor output is also observed to be increased almost linearly with the refractive index of the medium. As shown in Figure 3, the performance of the LRIS improves with an increase of the inclination angles. The larger the inclination angles of θ_1 and θ_2, the better the performance of liquid refractive index response.

Inset of Figure 3 shows the maximum normalized output of the sensor as a function of refractive index for various inclination angles. The normalized outputs were taken at the sensor probe position of 1.1, 2.0 and 3.4 mm for inclination angles of 20°, 10° and 0°, respectively, which is indicated by vertical dash lines in Figure 3. It was found that the sensitivities of the sensor increase with the increment of probe inclination angle. As shown in the inset of Figure 3, the highest sensitivity of 0.8235 is achieved by the use of probe with inclination angle of 20° which is almost 13 times higher than that in zero inclination. Figure 4 shows the simulation curves of the LRIS at various inclination angles for the receiving and transmitting fibers when the refractive index of liquid is set at 1.3. It is clearly seen that the inclination angle of receiving fiber θ_1 has the stronger affect in the sensor output compared with the angle θ_2. As shown in Figure 4, the highest output power is achieved by the inclination angles; $\theta_1 = 20°$ and $\theta_2 = 10°$. The lowest output power is observed when the inclination angles of θ_1 and θ_2 are set at 0° and 10°, respectively. These results show that the sensor sensitivity can be increased by increasing the inclination angle especially for θ_1. However, increasing the inclination is very difficult to be implemented in the experiment unless we can control the position of both fibers very precisely. Therefore, the angle cannot be increased to more than 20° in this work.

In our experiment, three different liquids: isopropyl alcohol, water and methanol are used as the surrounding medium at two conditions; zero inclination for both fibers and the same inclination angles of 10° for both fibers. The refractive index values for isopropyl alcohol, water and methanol are 1.377, 1.333 and 1.329, respectively. The performance of the sensor which uses air as the surrounding medium is also investigated for comparison purpose. During the experiment operation, the sensor probe is mounted onto the stage and the tank is fixed in the experiment table. The liquid in the tank is changed without moving the tank to ensure the accuracy of the measurement. The room temperature was kept at 28°C to ensure that the refractive index of the liquid is maintained and only displacement parameter is changed in the experiment.

Figure 5 shows the displacement curve at various surrounding media when the inclination angles are set at 0° for both transmitting and receiving fibers. As shown in this figure, the normalized peak output power increases from 0.83 to 1.00 as the refractive index increases from 1.329 (methanol) to 1.377 (alcohol). It is also found that the displacement position for the peak output increases from 4.0 to 5.1 mm as the refractive index increases from 1.329 to 1.377. This is attributed to the acceptance cone angle that increases as the refractive index increases. The larger acceptance angle provides a mean to collect more signal power. Figure 6 shows the displacement curves when the inclination angles for both fibers are set at 10°. As seen in Figure 6, the peak power and its position increase with the refractive index. The peak location of the curve also increases from 3.0 to 3.4 mm as the refractive index changes from 1.329 to 1.377. From these experimental results, it was found that the higher sensitivity for the sensor can

Figure 3 Simulation results for the displacement at various inclination angles and refractive indices

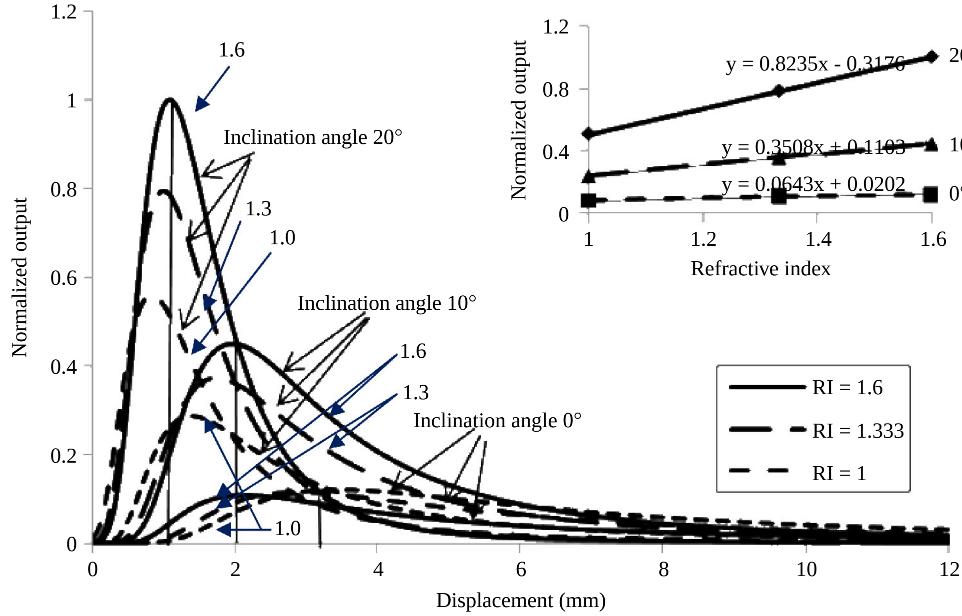

Note: Inset shows the maximum normalized output against the refractive index for inclination angles of 0°, 10° and 20°

Figure 4 The output power against displacement for various probe inclination angle combinations when the refractive index is set at 1.3

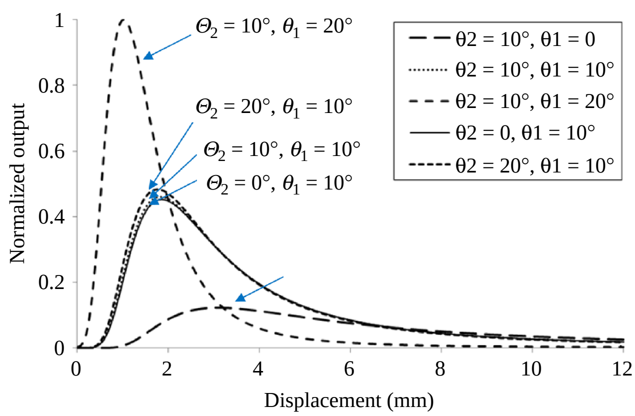

Figure 5 Experiment results of the displacement curve at various liquid materials when the probe inclination angles are set at 0°

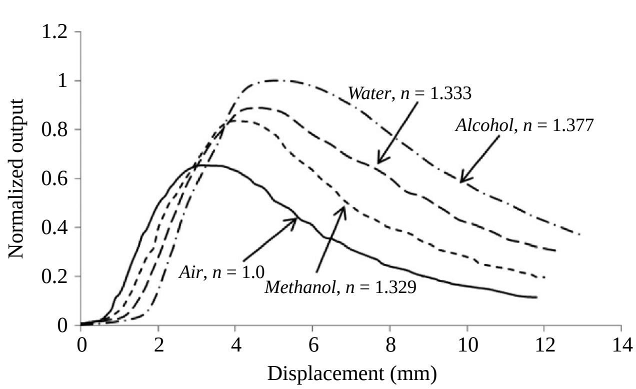

Figure 6 Experiment results of the displacement curve at various liquid materials when the probe inclination angles for both transmitting and receiving fibers are set at 10°

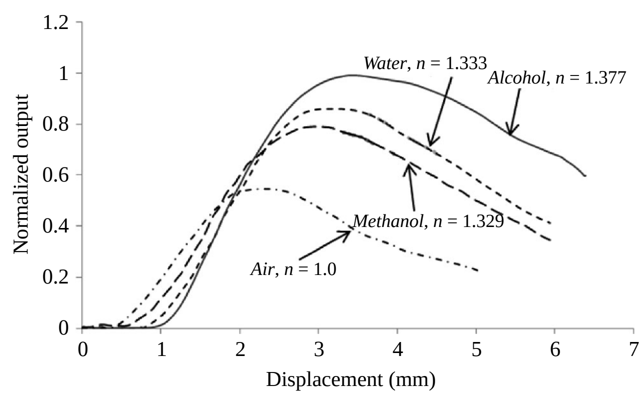

be achieved with the use of 10° inclined probe compared to that of straight probe. The sensitivities are obtained at 0.11/mm and 0.04/mm for the sensors with 10° and 0° inclination angles, respectively. This finding may be quite useful for chemical, pharmaceutical, biomedical and process control sensing applications.

5. Conclusion

A simple LRIS is theoretically and experimentally demonstrated using a pair type of bundle fiber which is inclined to increase the sensitivity. Through the theoretical analysis, a highest sensitivity can be achieved by using a probe inclined with angle 20° which is almost 13 times higher than that of the straight probe. Both theoretical and experimental results show that the peak power and the location of the displacement curve changes with refractive index. It was also found experimentally that the sensitivity of the sensor with 10° inclination of probe arrangement shows a higher sensitivity compared to that of the use of straight probe. The sensitivities are obtained at 0.11/mm and 0.04/mm for the sensors with 10° and 0° inclination angles, respectively.

References

Chaudhari, A.L. and Shaligram, A.D. (2002), "Multi-wavelength optical fiber liquid refracto-metry based on intensity modulation", *Sensor and Actuators A: Physical*, Vol. 100 Nos 2/3, pp. 160-4.

Kleiza, V. and Verkelis, J. (2007), "Some advanced fiber-optic amplitude modulated reflection displacement and refractive index sensors", *Nonlinear Analysis: Modelling and Control*, Vol. 12 No. 2, pp. 213-25.

Lim, K.S., Harun, S.W., Yang, H.Z., Dimyati, K. and Ahmad, H. (2009), "Analytical and experimental studies on asymmetric bundle fiber displacement sensors", *J. Modern Optics*, Vol. 56 No. 17, pp. 1838-42.

Nath, P., Singh, H.K., Datta, P. and Sarma, K.C. (2008), "All-fiber optic sensor for measurement of liquid refractive index", *Sensor and Actuators A: Physical*, Vol. 148 No. 1, pp. 16-18.

Rastogi, P.K. (1997), *Optical Measurement Techniques and Applications*, Artech House, Boston, MA.

Suhadolnik, A., Babnik, A. and Mozina, J. (1995), "Optical fiber reflection refractometer", *Sensor and Actuators B: Chemical*, Vol. 29, pp. 428-32.

Yang, H.Z., Harun, S.W. and Ahmad, H. (2009), "Fiber optic displacement and liquid refractive index sensors with two asymmetrical inclined fibers", *Sensors and Transducers Journal*, Vol. 108 No. 9, pp. 80-8.

Yasin, M., Harun, S.W., Abdul-Rashid, H.A., Kusminarto, K. and Ahmad, H. (2007), "The performance of a fiber optic displacement sensor for different types of probes and targets", *Laser Physics Letters*, Vol. 5 No. 1, pp. 55-8.

Yasin, M., Harun, S.W., Kusminarto, K., Zaidan, A.H., Thambiratnam, K. and Ahmad, H. (2009), "Design and operation of a concentric-fiber displacement sensor", *Fiber and Intergrated Optics*, Vol. 28 No. 4, pp. 301-9.

Corresponding author

S.W. Harun can be contacted at: swharun@um.edu.my

To purchase reprints of this article please e-mail: **reprints@emeraldinsight.com**
Or visit our web site for further details: **www.emeraldinsight.com/reprints**

Research article

Theoretical and experimental studies on concave mirror-based fiber optic displacement sensor

H.Z. Yang
Photonics Research Center, University of Malaya, Kuala Lumpur, Malaysia

S.W. Harun
Photonics Research Center, University of Malaya, Kuala Lumpur, Malaysia and
Department of Electrical Engineering, University of Malaya, Kuala Lumpur, Malaysia, and

H. Ahmad
Photonics Research Center, University of Malaya, Kuala Lumpur, Malaysia

Abstract

Purpose – The purpose of this paper is to investigate, theoretically and experimentally, a concave mirror-based fiber optic displacement sensor performance for three-axes directional measurements.

Design/methodology/approach – Mathematical model is constructed based on spherical mirror properties of the concave mirror and the simulated result is found to be in good agreement with the experimental results.

Findings – Both theoretical and experimental results show that the focal length and radius of the concave mirror make significant influence to the displacement response. In the *x*-axes measurement, six linear slopes are obtained with four of them are located in the vicinity of the position, two times of the focal length. The maximum measurement range of about 20 mm is obtained using a focal length of 10 mm. In the *y*- and *z*-axes displacement measurements, the linear range increases as the diameter of concave mirror increases. The longest linear range of 8 mm is achieved at mirror radius of 10 mm.

Originality/value – This is the first demonstration of three axes directional displacement measurements using a concave mirror as a target

Keywords Fiber optic sensors, Mathematical modelling, Simulation

Paper type Research paper

1. Introduction

In general, there are two types of fiber optic displacement sensors (FODS); namely interferometry- and intensity modulation-based FODS. FODS are employed to control the distance, vibration and position, etc. in monitoring systems. The interferometry-based FODS are operated by combining two different path light waves where one is the measurement wave and the other is the reference wave to generate interference fringes that are used to measure the position shift (Rastogi, 1997). The interferometry-based displacement sensor can provide ultrahigh precision displacement control; however, it requires complicated instruments and therefore incurs high cost along with having limited bandwidth in comparison to intensity modulation-based FODS. The intensity modulation-based FODSs on the other hand are capable of using low-cost components to achieve high bandwidth and ultrahigh precision displacement control (Muephy and Coursolle, 1990; Golnabi, 2000; Harun *et al.*, 2009; Lim *et al.*, 2009). Most FODSs employ a multimode plastic optic fiber as a probe and a flat mirror as a reflective target, and a detector is used to measure the intensity of the reflected light (which the amount is a function of displacement). Work on FODS systems currently focus on improving the performance of the FODS such as enhancing the dynamic range and increasing sensitivity using a variety of sensor probe, reflector and laser source arrangements (Golnabi and Azimi, 2008; Huang and Tata, 2008; Cao *et al.*, 2007). However, for potential industry applications, there is a requirement for multi-axes displacement sensing in the vibration, position and strain monitoring system (Sagrario and Mead, 1998). This presents a problem as conventional FODSs are normally designed to measure the displacement in one axes; it is shrivelled for other two axes.

Recently, a new FODS was proposed using a pair type of bundle fiber as a probe and a concave mirror as a target to provide at least six elective sensitivities and linear ranges (Yang *et al.*, 2009; Harun *et al.*, 2009, 2011). The theoretical analysis has shown that the performance of sensor is affected

The current issue and full text archive of this journal is available at
www.emeraldinsight.com/0260-2288.htm

Emerald

Sensor Review
31/1 (2011) 65–69
© Emerald Group Publishing Limited [ISSN 0260-2288]
[DOI 10.1108/02602281111099107]

by many parameters such as focal length and diameter of concave mirror. In this paper, the concave mirror-based FODS is analysed further to demonstrate three-dimensional measurement in order to meet the industrial demand for the multi-axes displacement sensor. The operational principles, mathematical analysis, software simulation and experiment setup for the proposed sensor are described in this paper.

2. Operational principle and theoretical analysis

The structure of the proposed sensor is shown in Figures 1 and 2 for *x*- and *yz*-axes measurements, respectively. As shown in both figures, the initial position of sensor probe tip should be located at the highest point of the concave mirror surface so that the three-axes displacement sensing can be achieved. The longitudinal axis of the transmitting fiber core should also be aligned so that it is co-axes with the normal axis of the concave mirror. To maximise the light-coupling efficiency, the sensor probe tip should be located as close as possible to the surface of concave mirror. The transmitting fiber works to carry the light from the laser source to the concave mirror. The light is then reflected and focused by the concave mirror so that it can be collected by the receiving fiber. The amount of the collected light varies with the displacement of the mirror in the axial direction *x* (Figure 1) as well as *y*, *z*- directions (Figure 2). The axial displacement is carried out in both positive and negative directions while other displacements in *y*- and *z*-axes are only done in one direction. Owing to the spherical reflective surface of concave mirror, the proposed sensor shows the same response characteristics for both displacement measurements in *y*- and *z*-axes.

As shown in Figure 1, the laser source emits light at an original point O which is situated in the transmitting fiber and at a distance of z_a from the fiber surface end. After the reflection in the concave mirror, the reflected laser source is concentrated at point O′ and virtually becomes another emitting point source. In the theoretical analysis of axial (*x*-axis) displacement, we assume that the intensity of the light emitted from the transmitting fiber can be well described with Gaussian distribution and the far field model are used in the point of laser source. In consideration of the limited reflecting surface area and focal length of the concave mirror, the transfer function of the proposed sensor in *x*-axis is given by Cao *et al.* (2007):

Figure 1 The structure of proposed sensor in the sensing displacement of *x*-axis

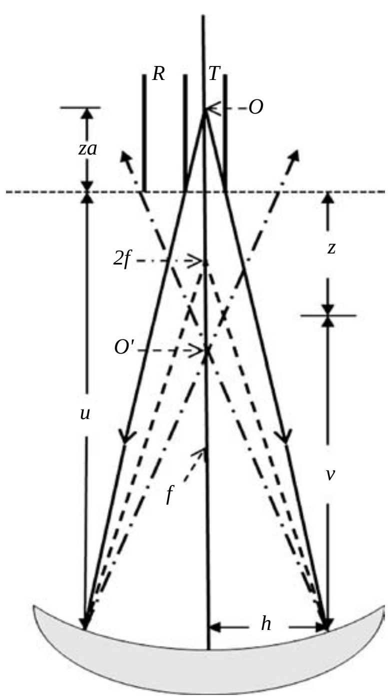

Figure 2 The structure of proposed sensor in the sensing displacement of *y*- and *z*-axes

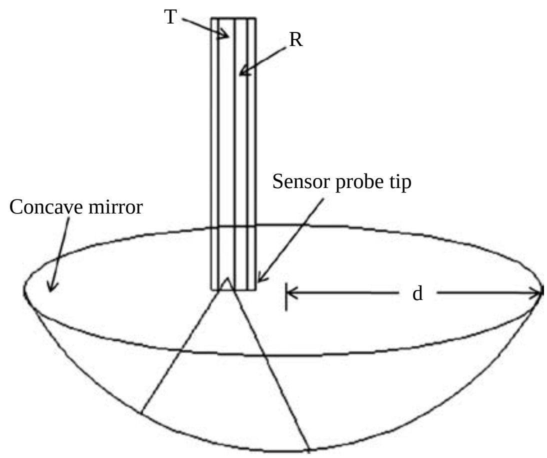

Note: T and R are the transmitting and receiving fibers, respectively

$$P(u) = \frac{2z_a^2 P_E\{1-\exp-(D^2/2(u+z_a)^2\theta^2)\}}{[u-((u+z_a)f/(u-f+z_a))]^2(((u+z_a)/f)-1)^2}\exp\left(-\frac{8z_a^2}{[u-((u+z_a)f/(u-f+z_a))]^2(((u+z_a)/f)-1)^2}\right) \tag{1}$$

where P_E is the emitting power of laser source, u is the distance between the sensor probe tip and concave mirror. The transfer function represents the receiving light power at the receiving fiber. The angle $\theta = \sin^{-1}(NA)$ where NA is the numerical aperture of the transmitting fiber. Equation (1) shows that the transfer function of proposed sensor in *x*-axis is governed by two important parameters, namely the focal length f and the diameter of the circular concave mirror D.

In earlier work (Muephy and Coursolle, 1990) employed a pair type bundle fiber and a graded index lens to measure the displacement. This sensor shows that the coupled power between the two fibers is approximately proportional to the amount of overlap area of the transmitting fiber and receiving fiber, and is a function of the relative lateral displacement between the fibers. In this work, a concave mirror, which has a similar function with the graded index lens to reflect and focus the incoming light is used. Therefore, the normalized transmittance function of Muephy and Coursolle (1990) can be used to study our sensor assuming that intensity distribution at the output plane of the transmitting fiber is uniform. The normalized transmittance function is given by:

Sensor Review
Volume 31 · Number 1 · 2011 · 65–69

$$T(d) = \frac{2}{\pi}\left\{\cos^{-1}\left(\frac{2d}{r_d}\right) - \left(\frac{2d}{r_d}\right)\left[1-\left(\frac{2d}{r_d}\right)^2\right]^{1/2}\right\} \quad (2)$$

where d is concave mirror displacement in y- or z- directions, r_d is the diameter of fiber core. It describes the coupled power between the transmitting and receiving fiber, which is strongly depended on the overlap area.

3. Experiment setup

Figure 3 shows the experimental setup of the proposed sensor for three-dimensional measurements. It consists of a He-Ne laser, an external chopper, a pair type of bundle fiber, a concave mirror and a silicon detector. The light source operates at wavelength of 594 nm with an average output power of 3.0 mW, beam diameter of 0.75 mm and beam divergence of 0.92 mRads. The chopper is used to modulate the light at a frequency of 200 Hz before launched into the transmitting fiber. A concave mirror is located at the output end of transmitting fiber to reflect and focus the transmitted light into a receiving fiber which is bundled together with the transmitting fiber. The receiving fiber routes the light into the photo detector which converts the light power into voltage. A lock-in amplifier is connected with the chopper and photo detector to act as a data-acquisition system and functions to match the phase between the modulation light and modulator chopper and removes the noise generated by laser source, photo detector and amplifier (Huang and Tata, 2008).

One of the major difficulties encountered during the experiment is the alignment of sensor probe and concave mirror as discussed in earlier section. The sensor probe should be vertically aligned with the focal point of the concave mirror. A translation stage is used in the experiment to provide multi-axial displacement control for alignment. The displacement measurement of x-axis is implemented by fixing the other two axes and ensuring that the longitudinal axis of the transmitting fiber is co-axis with the normal axis which is also located at the center of the concave mirror. In the displacement measurement for the y- and z-axes, the sensor probe alignment in x-axis is fixed as shown in Figure 2. The mathematical model of the sensor is simulated using MATLAB programming. The following parameters are used in the calculations; the wavelength of the laser source $\lambda = 594$ nm, numerical aperture value $NA = 0.35$ and fiber core radius of 0.25 mm. The performances of the sensor are investigated for different focal length and concave mirror diameters. The focal length and diameter is varied from 6-10 mm and 12-20 mm, respectively.

Figure 3 Experimental setup for the proposed FODS with a concave mirror

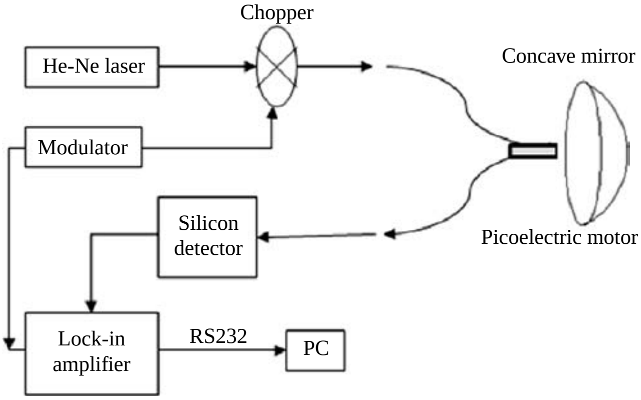

4. Results and discussions

Figures 4 and 5 show the experimental and theoretical displacement results of the FODS in x- and y-axes, respectively. The theoretical results are obtained by fitting of theoretical analysis in equations (1) and (2). In the experiment and calculation, the pair-type bundle fiber with core diameter of 0.5 mm is used while the focal length, radius and height of concave mirror are fixed at 6, 6 and 1.5 mm, respectively. The positive and negative portions in Figure 4 show the situation where sensor probe is moving farer and closer, respectively, towards the concave mirror. As shown in Figure 4, there are six linear slopes in the displacement response and four of them are located in the vicinity of $u = 2f$ which is a function of the concave mirror focal length as described in equation (1). The results comparison made in Figure 5 are normalized in both displacement and output power. From equation (2), the displacement is normalized by $2u/r_d$. In this sensor, the probe is located as close as possible to the horizontal surface of concave mirror which results in the receiving fiber not being able to collect the reflected light as the sensor probe is moving to the fringe of concave mirror. Thus, there is a blind

Figure 4 The results comparison of theoretical and experiment in *x*-axis

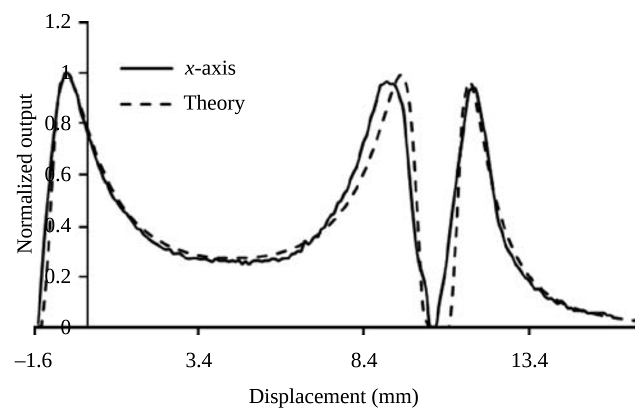

Figure 5 The results comparison of theoretical and experiment in *y*-axis

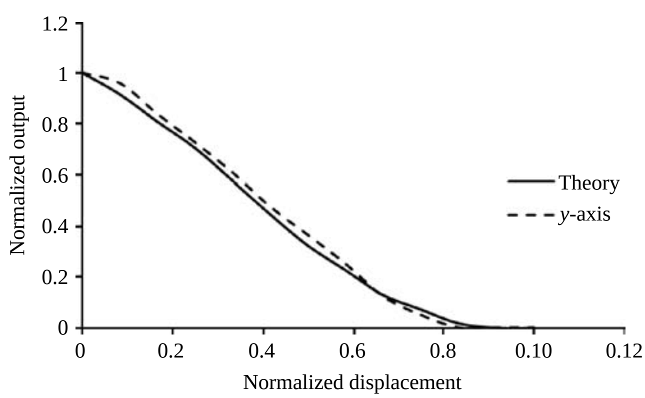

region in the normalized displacement of 0.83-1. Figure 6 shows the displacement curves between y- and z-axes measurements. As a result of the blind region in the displacement measurement of y- and z-axes, the linear range of proposed sensor is set to be 5 mm which is smaller than radius of concave mirror of 6 mm as shown in Figure 6. In this figure, the same displacement responses are achieved in both y- and z-axes because of the sphere reflective surface of concave mirror as explained in the previous section.

Figure 7 shows the displacement response in x-axis at various focal lengths of the concave mirror. The radius of the concave mirror used in this experiment is 6 mm while the heights of the concave mirror are 1.50, 1.25 and 1.00 mm for the focal lengths of 6, 8 and 10 mm, respectively. As shown in Figure 7, the power intensity is at the minimum at a position of approximately -1.5 mm from the initial probe position and as the power increases; it reaches its maximum value and reduces as the displacement increases. Then, the displacement response reaches another two maximum points which are located sandwiching the point at 2f, where f is the focal length of the mirror. This property enables flexible sensing based on displacement range of interest by properly choosing the desired focal length. The maximum measurement range about 20 mm is obtained using a focal length of 10 mm. Figure 8 shows the normalised output of the sensor against the displacement in the y-axis at various concave mirror radii. In the experiment, the focal length is fixed at 10 mm and the heights of mirror are measured to be 1, 2 and 3 mm when the radius is set at 6, 8 and 10 mm, respectively. The maximum received power is increased by three times as the radius of concave mirror radius decreases from 10 to 6 mm. As shown in Figure 8, the linear range of the sensor increases as the diameter of concave mirror increases. The longest linear range of 8 mm is achieved at a mirror radius of 10 mm. Future research works should be focused on finding new application to this sensor.

Figure 6 Experiment results of displacment responses of y- and z-axes

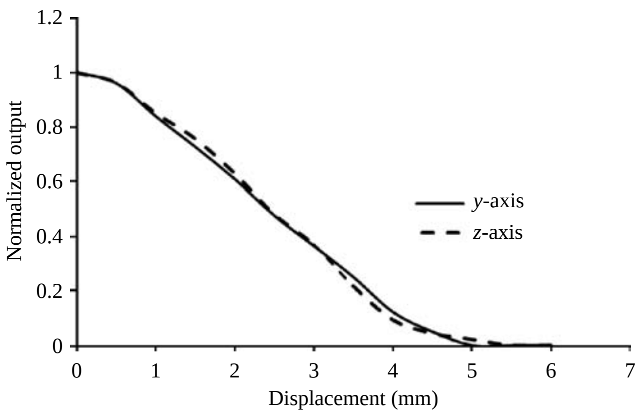

Figure 7 Displacement response of the sensor in x-axis at different focal lengths: 6, 8 and 10 mm

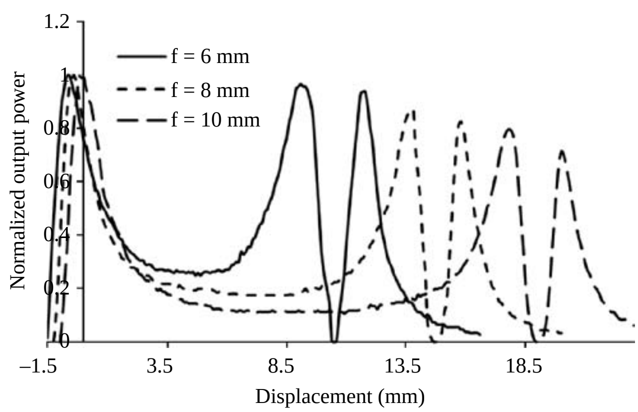

Figure 8 Displacement response of the sensor in y-axis at different radius of concave mirror: 6, 8 and 10 mm

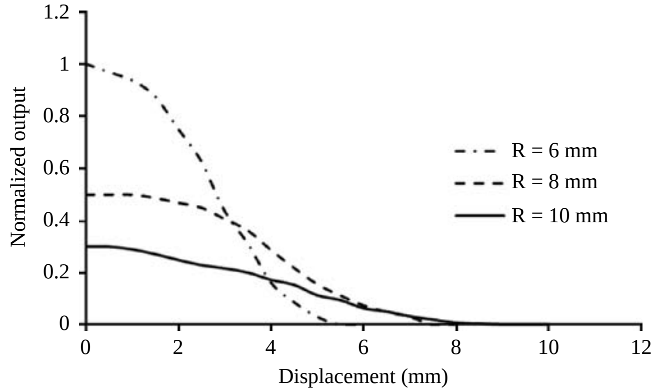

5. Conclusion

A three-axes directional displacement sensing is demonstrated using a concave mirror in conjunction with a pair type bundle fiber as a probe. A mathematical model is constructed based on spherical mirror properties of the concave mirror and the simulated result is found to be in good agreement with the experimental results. Both the theoretical and experimental results show that the focal length and radius of the concave mirror make a significant influence to the displacement response. The displacement curve for the x-axis measurement has three maximum points with the second and third maximum points sandwiching the point at 2f, where f is the focal length of the mirror. A measurement range of approximately 20 mm is obtained using a focal length of 10 mm. In the y- and z-axes displacement measurements, the light intensity almost linearly decreases with the distance. The linear range increases as the diameter of concave mirror increases with the longest linear range of 8 mm is achieved at mirror radius of 10 mm.

References

Cao, H.M., Chen, Y.P., Zhou, Z.D. and Zhang, G. (2007), "Theoretical and experimental study on the optical fiber bundle displacement sensors", *Sensor and Actuators A*, Vol. 136, pp. 580-7.

Golnabi, H. (2000), "Fiber optic displacement sensor using a coated lens optic", *Review of Science Instruments*, Vol. 71, pp. 4314-8.

Golnabi, H. and Azimi, P. (2008), "Design and operation of a double-fiber displacement sensor", *Optics Communications*, Vol. 281, pp. 614-20.

Harun, S.W., Yang, H.Z. and Ahmad, H. (2011), "Theoretical and experimental studies on liquid refractive index sensor based on bundle fiber", *Sensor Review*, accepted for publication, Vol. 31 No. 1, pp. pp. 65-9.

Harun, S.W., Yang, H.Z., Yasin, M. and Ahmad, H. (2009), "Theoretical and experimental study on the fiber optic displacement sensor with two receiving fibers", *Microwave and Optical Technology Letters*, Vol. 52, pp. 373-5.

Harun, S.W., Yang, H.Z., Lim, K.S., Tamjis, M.R., Dimyati, K. and Ahmad, H. (2009), "Fiber optic displacement sensor based on concave mirror", *Optoelectronics and Advanced Materials-Rapid Communications*, Vol. 3, pp. 1139-41.

Huang, H.Y. and Tata, U. (2008), "Simulation, implementation, and analysis of an optical fiber bundle distance sensor with single mode illumination", *Applied Optics*, Vol. 47 No. 9, pp. 1302-9.

Lim, K.S., Harun, S.W., Yang, H.Z., Dimyati, K. and Ahmad, H. (2009), "Analytical and experimental studies on asymmetric bundle fiber displacement sensors", *Journal of Modern Optics*, Vol. 56, pp. 1838-42.

Muephy, P.J. and Coursolle, T.P. (1990), "Fiber optic displacement sensor employing a graded index lens", *Applied Optics*, Vol. 29, pp. 544-7.

Rastogi, P.K. (1997), *Optical Measurement Techniques and Applications*, Artech House, Boston, MA.

Sagrario, D. and Mead, P. (1998), "Axial and angular displacement fiber-optic sensor", *Applied Optics*, Vol. 37, pp. 6748-54.

Yang, H.Z., Harun, S.W. and Ahmad, H. (2009), "Fiber optic displacement and liquid refractive index sensors with two asymmetrical inclined fibers", *Sensor and Transducer*, Vol. 108, pp. 80-8.

Corresponding author

S.W. Harun can be contacted at: swharun@um.edu.my

To purchase reprints of this article please e-mail: **reprints@emeraldinsight.com**
Or visit our web site for further details: **www.emeraldinsight.com/reprints**

Sensors & Transducers Journal, Vol. 108, Issue 9, September 2009, pp. 80-88

Sensors & Transducers

ISSN 1726-5479
© 2009 by IFSA
http://www.sensorsportal.com

Fiber Optic Displacement and Liquid Refractive Index Sensors with Two Asymmetrical Inclined Fibers

[1]H. Z. Yang, [2]S. W. Harun and [1]H. Ahmad
[1]Photonics Research Center, University of Malaya 50603 Kuala Lumpur, Malaysia
[2]Dept. of Electrical Engineering, University of Malaya, 50603 Kuala Lumpur, Malaysia
E-mail: swharun@um.edu.my

Received: 22 June 2009 /Accepted: 21 September 2009 /Published: 28 September 2009

Abstract: Fiber optic displacement sensor (FODS) with two asymmetrical inclined fibers is studied theoretically and experimentally. A liquid refractive index sensor (LRIS) is then demonstrated using the similar sensor set-up. The theoretical result of the FODS is in good agreement with the experimental result, verifying the feasibility of our theoretical model. The performance of FODS is strongly depended on core radius and diameter of fibers used as well as inclination angle of two asymmetrical fiber core. The maximum sensitivities of 0.2752, 0.3759 and 0.7286 mV/μm are obtained at inclination angles of 10°, 20° and 30°, respectively. Meanwhile, the maximum linear ranges of 10.4 mm, 7 mm and 3 mm are obtained at inclination angles of 10°, 20° and 30°, respectively. The proposed LRIS produces the highest output different for increase in refractive index at displacement of 3.3 mm. At this distance, the output intensity increases almost linearly as a function of refractive index of the medium. *Copyright © 2009 IFSA.*

Keywords: Fiber-optic displacement sensor, Liquid refractive index sensor, Fiber-optic sensor

1. Introduction

Intensity modulation is one of the important methods that is normally used for displacement measurement in conjunction with multimode fiber. The fiber optic displacement sensor (FODS) has inherited many advantages such as virtues of simplicity, reliability and low cost [1]. To date, many works have been reported on the intensity modulation based FODS [2-5], which the probe consists of a pair of fibers used for transmitting and receiving the light. For instance, Buchade, et. al. [4] presented a FODS using two fibers inclined with a same angular angle and reported the sensitivity was enhanced compared with the conventional sensor with parallel bundled fibers. It also reported that the performances of the FODS with two fibers are depended mainly on four parameters: the offset, the lateral separation and the angle between the transmitting and receiving fiber tips, and the angle of the reflector [6]. However, there is still a lack of research work on the FODSs with different geometry of the receiving fiber.

Another important fiber optic sensor is a liquid refractive index sensor (LRIS), which is vital to design of optical instruments and is also a great value in chemical applications. The knowledge of refractive index of a substance is useful in indentifying and determining the concentration of organic substances. The refractive index of liquid samples can be measured in many ways such as implementation of total internal reflection and prism coupling techniques [7-9]. For instance, Nath, et al [9] proposed a liquid refractive sensor based on the frustrated total internal reflection effect caused by refractive index change of a medium surrounding one optical fiber tip.

In this paper, a mathematical model for the intensity modulation FODS with two asymmetrical and inclined fibers is developed. The developed model is used to simulate the response of the sensor with different inclined fiber angles. Experimental validation of simulated results on the inclined fiber sensor is also carried out in this study. In this work, a new LRIS is also proposed using the similar set-up to detect a refractive index of liquid media. The liquid of which the refractive index is measured is filled up in the gap between probe and reflector. Depending upon the refractive index of liquid, angle of emittance will change which will affect the received output power by receiving fiber.

2. Sensor Design and Theoretical Analysis

Fig. 1 shows the geometry of the inclined displacement sensor, which consists of a transmitting fiber, receiving fiber and a reflector. The sensor performance is studied at various core radiuses of transmitting and receiving fiber. Fig. 1(a) (Fig. 1(b)) shows the geometry of the sensor in case of the receiving core is bigger (smaller) than the transmitting core. Two asymmetrical transmitting and receiving fibers are mounted at an angle 'θ' with reference to the normal to the reflector. This ensures the receiving fiber core to collect the maximum power from emitting light cone of the transmitting fiber. The shortest distances between the sensor probe tips and reflector are x_1 and x_2 for transmitting fiber and receiving fiber, respectively. The dash lines inside the receiving fiber represents the size of the transmitting fiber. The image of transmitting (receiving) fiber is formed at a further distance x_1 (x_2) opposite to the transmitting (receiving) fiber beyond the reflector. The image fiber is thus seen located at $2x_1$ or $2x_2$ from the original position of the probe. Effectively the reflected light appears to form a cone and reaches the receiving fiber, which is parallel aligned in the cone as shown in Fig. 1.

As shown in Fig. 1, the core radius of the transmitting and receiving fibers are denoted as r_1 and r_2, respectively. Meanwhile, the diameters of transmitting fiber and receiving fiber are r_{d1} and r_{d2}, respectively. We assume that the ratio between the core radius of two fibers is k_1, $k_1 = r_1/r_2$ and the ratio of fiber diameter of the two fibers is $k_2 = r_{d1}/r_{d2}$. From the geometry analysis of Fig. 1, the distance between the two sides of image of transmitting and receiving fibers is given by:

$$f = \left| r_{d1} \times \cos(2\theta) - 2x_1 \times \sin(\theta) \right| \quad (1)$$

Then, the distance between two fiber core, D is obtained as:

$$D = f + \frac{r_{d2} - r_{d1}}{2} = f + \frac{r_{d2}(1-k_2)}{2} \quad (2)$$

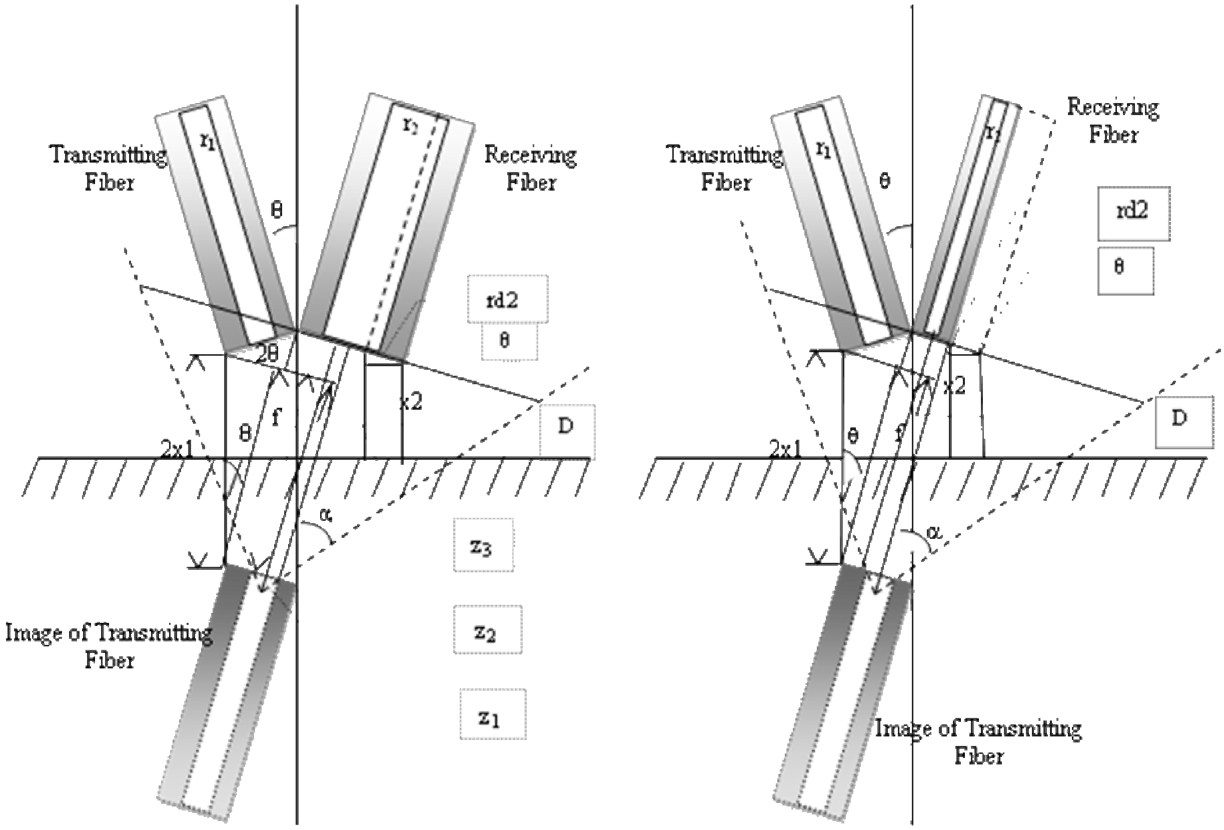

(a) $r_2>r_1$ (b) $r_2<r_1$

Fig. 1. The structure of sensor probes (a) $r_2>r_1$; (b) $r_2<r_1$.

The acceptance angle of transmitting fiber, α is given by $\alpha = \sin^{-1}(\frac{NA}{n})$, where NA is a numerical aperture for the transmitting fiber. The distance between emitting points of transmitted light to the receiving flat core is denoted as z, which is given by:

$$z = z_1+z_2+z_3\,, \tag{3}$$

where $z_1 = r_1\times\cot\alpha = k_1r_2\times\cot\alpha$, $z_2 = 2x_1\times\cos(\theta)$ and $z_3 = r_{d1}\times\sin(2\theta) = k_2r_{d2}\times\sin(2\theta)$ as illustrated in Fig. 1.

To analyze the power collected by the receiving fiber, we simply analysis the light inside the fiber by using a Gaussian beam approach. The irradiance of emitted light is obeying an exponential law according to

$$I(r,z) = \frac{2P_E}{\pi\omega^2(z)}\exp\left(-\frac{2r^2}{\omega^2(z)}\right), \tag{4}$$

where P_E is the emitted power from the light source, r is the radial coordinate and z is the longitudinal coordinate calculated by equation (3). $\omega(z)$ is the beam radius which is also a function of z, $\omega(z) = \omega_0\sqrt{1+\left(\frac{z}{z_R}\right)^2}$. The waist radius ω_0 and Rayleigh range z_R are the important parameters in the

Gaussian Beam function. The optical power received by the receiving fiber can be evaluated by integrating the irradiance, I over the surface area of the receiving fiber end, S_{r_2}

$$P(r,z) = \int_{S_{r_2}} I(r,z)dS_{r_2} \tag{5}$$

To simulate conveniently, the Equation (5) can be described in other expressions;

$$P(k_1,k_2,z) = \frac{2P_E}{\pi w^2(z)} \int_{y=-r_2}^{r_2} \int_{x=D-\sqrt{r_2^2-y^2}}^{D+\sqrt{r_2^2-y^2}} \exp\left(-\frac{2(x^2+y^2)}{w^2(z)}\right)dxdy \tag{6}$$

The $P(k_1,k_2, z)$ is the power collected by the receiving fiber corresponding the parameters k_1 and k_2. The radial coordinate r is expressed by $\sqrt{x^2+y^2}$ in Cartesian coordinate system.

Fig. 2 illustrates the overlap area of the reflected light area and the core of the receiving fiber. The overlap area is zero at $x_2 = 0$ (Fig. 1(a)) or $x_1 = 0$ (Fig. 1(b)) and at a very small displacement (blind area) where the jacket of the two fibers blocks the reflected light. As the displacement is increased further, the overlap area increases and thus increases the total power collected by the receiving core. The total power is maxima when the reflected light cone covers the entire receiving core area. After that, the received optical power starts to decay exponentially as the displacement continues to increase. The received optical power is strongly dependent on the core size of the receiving fiber. At inclination angle of 2θ between the transmitting and receiving fibers, the distance x_1 between the sensor probe tip and reflector is given by [4]

$$x_1 = \frac{r_{d1}}{2}(cosec\theta - 2sin\theta) \tag{7}$$

From the geometrical analysis of Fig. 1, the distance x_2 is obtained as; $x_2 = x_1 - r_{d3}\sin\theta$ for $r_{d1} < r_{d2}$ (Fig. 1 (a)) or $x_2 = x_1 + r_{d3}\sin\theta$ for $r_{d1} \geq r_{d2}$ (Fig. 1(b)) where $r_{d3} = r_{d2} - r_{d1}$. Therefore, the distance between sensor probe tip and reflector mirror can be summarized as;

$$\begin{aligned} x_2 &= \frac{r_{d2}}{2}[\, k_2 cosec\theta + 2sin\theta(1-2k_2)] \quad (r_{d1} > r_{d2}) \\ &= \frac{k_2 r_{d2}}{2}(\, cosec\theta - 2sin\theta) \quad (r_{d1} = r_{d2}) \\ &= \frac{r_{d2}}{2}(\, k_2 cosec\theta - 2sin\theta) \quad (r_{d1} < r_{d2}) \end{aligned} \tag{8}$$

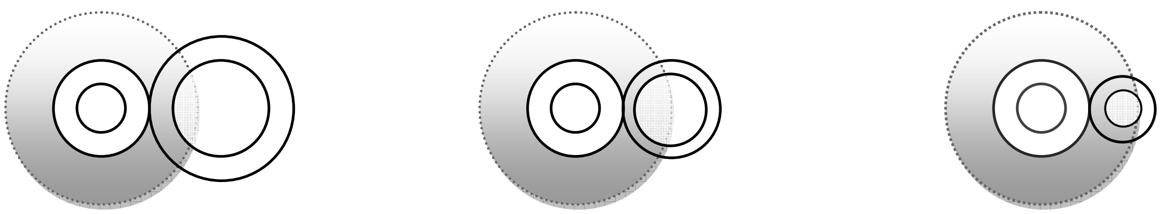

(a) $r_{d1} < r_{d2}$ (b) $r_{d1} = r_{d2}$ (c) $r_{d1} > r_{d2}$

Fig. 2. Overlap area view (a) $r_{d1} < r_{d2}$; (b) $r_{d1} = r_{d2}$; (c) $r_{d1} > r_{d2}$.

3. Simulation and Experiment

The proposed sensor is simulated by using a MATLAB programming. To simplify the analysis, the k_1 values of 0.5, 0.667, 1, 1.5 and 2 are used. The k_2 value is set based on the availability of the fiber in our laboratory. In this simulation, the k_2 values of 0.5, 1 and 2 are used. The wavelength of the laser source λ is set at 594 nm. The numerical aperture values $NA_1 = 0.27$, $NA_2 = 0.32$ and $NA_3 = 0.4$ are used for the core radius of 0.25 mm, 0.5 mm and 0.75 mm, respectively.

To verify the simulated results the FODS is constructed by mounting the transmitting and receiving fibers on the plastic board at angle θ with reference to the normal of the reflector. Separate samples with various fiber diameters and core radius are prepared for angle $\theta = 10^o$, 20^o and 30^o. Light from 594 nm He-Ne laser is modulated by an external chopper at frequency of 200 Hz and launched into the transmitting fiber. The light has an average output power of 3.0 mW, beam diameter of 0.75 mm and beam divergence of 0.92 mrads. The length of transmitting and receiving fiber length is approximately 2 m. The transmitting fiber radiates the modulated light from the light source to the target mirror, while the displacement of sensor probe tip between mirror is controlled by a piezoelectric & driver. The reflective light from target mirror, which is mounted in the bottom of tank, is collected by the receiving fiber whose carries the light into the silicon detector. A lock-in amplifier is connected with the detector to reduce the dc drift voltage due to an ambient light. The initial experiment is carried out by varying the inclination angle between the fibers. The liquid of which the refractive index is measured is filled up in the tank for the LRIS application. The experiment setup of the FODS and LRIS is shown in Figure 3.

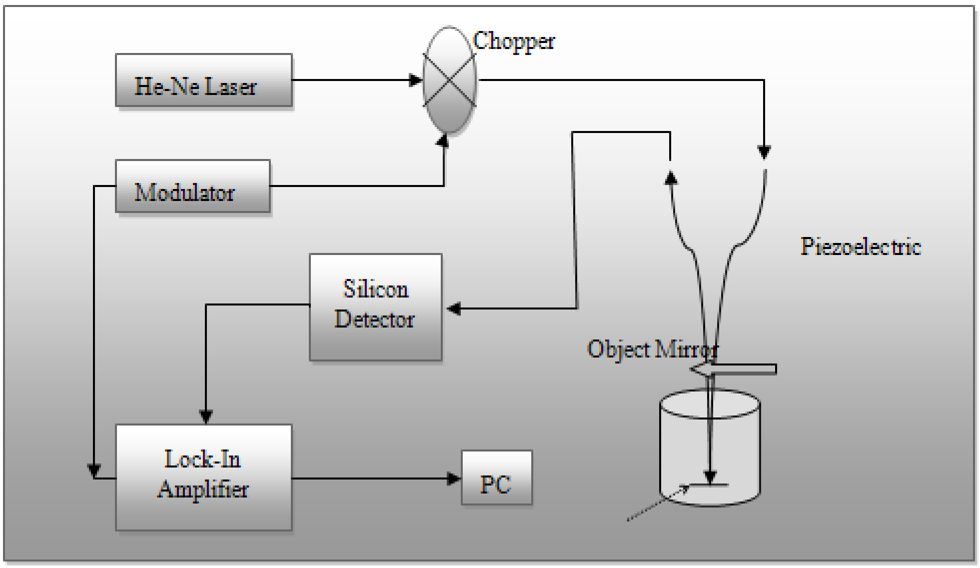

Fig. 3. Experiment setup of the FODS and LRIS.

4. Result and Discussion

Fig. 4 compares the experimental and theoretical plots of the normalized output collected against normalized displacement between probe and reflector with air medium in between. In this study, the ratios k_1, k_2, and angle θ are set at 0.667, 0.5, 10° respectively. As shown in the figure, the theoretical curve is in good agreement with the experimental curve, verifying the feasibility of our theoretical model. It is also observed that up to 0.3 (0.5) of separation distance for experimental (theoretical) curve, light in transmitting fiber would be reflected back into itself and little or no light would be transferred to receiving fiber. This is then referred to as the blind region. As the distance increases, the reflected cone overlaps the receiving fiber core and hence the output intensity increases. This relation is continued until the entire face of receiving fiber is illuminated with the reflected light. This point is called optical peak and corresponds to maximum voltage. As the gap increases beyond this transition region, the intensity drops off following roughly an inverse-square law. The small discrepancy between the theoretical and experimental results is due to the noise sources such as shot noise and thermal noise, which are added to the value of the experimental results and are not calculated in the theoretical analysis.

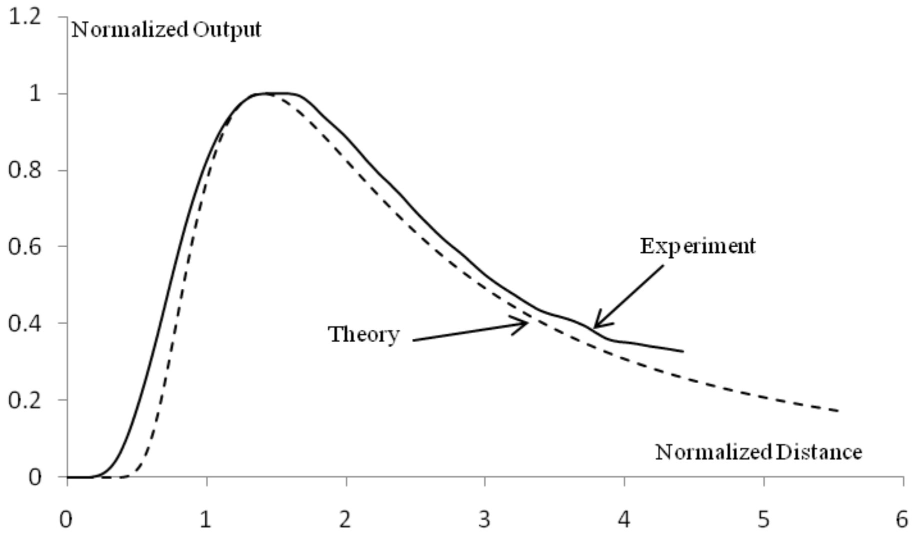

Fig. 4. Comparison between theoretical and experimental curves of the FODS with air medium in between the gap.

The experiments are also carried out to study the effect of k_1 and k_2 values as well as angle θ on the performance of FODS. Fig. 5 shows the normalized output power against displacement for the FODS at various k_1 and k_2 values as well as the inclination angle. Figs. 5 (a), (b) and (c) show the curves at 10°; $20^{\circ}$and 30° respectively with an air gap in between the displacement. By comparing the curves in Fig. 5, we understand that the performance of FODS is strongly depended on the fiber core size. The output power collected by receiving fiber is highest when the k_1 and k_2 values are set at 0.667 and 1, respectively. The inclination angle θ of two asymmetrical fiber core is also effected the sensor performance with the bigger inclined angle has a higher output sensitivity with a lower linearity range. Compared to the FODS with zero inclination angle, the sensitivity of the proposed sensor increased by 3.6, 8.5 and 16 times with the inclination angles of 10°, 20° and 30°, respectively. However, the corresponding linear ranges are reduced by 67 %, 55 % and 33 %, respectively. The performances of the proposed FODS are summarized as shown in Table 1. By using the k1 and k2 values of (0.667, 1), the maximum sensitivities of 0.2752 mV/μm, 0.3759 mV/μm and 0.7286 mV/μm are obtained at inclination angles of 10°, 20° and 30°, respectively. This sensitivity is higher compared to the previous work by Buchade, et. al [4]. The maximum linear ranges of 10.4 mm, 7 mm and 3 mm are obtained at inclination angles of 10°, 20° and 30°, respectively for the FODS with k_1 and k_2 values of (0.667, 1).

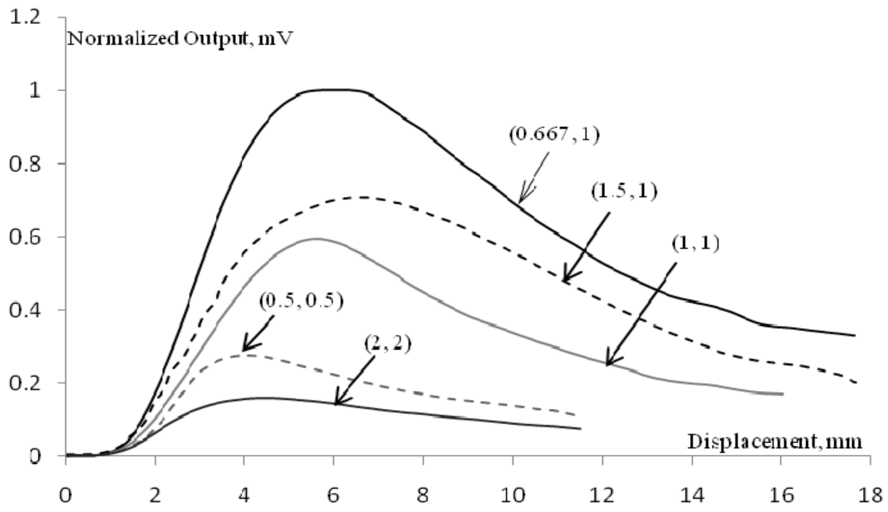

(a) at 10° angle

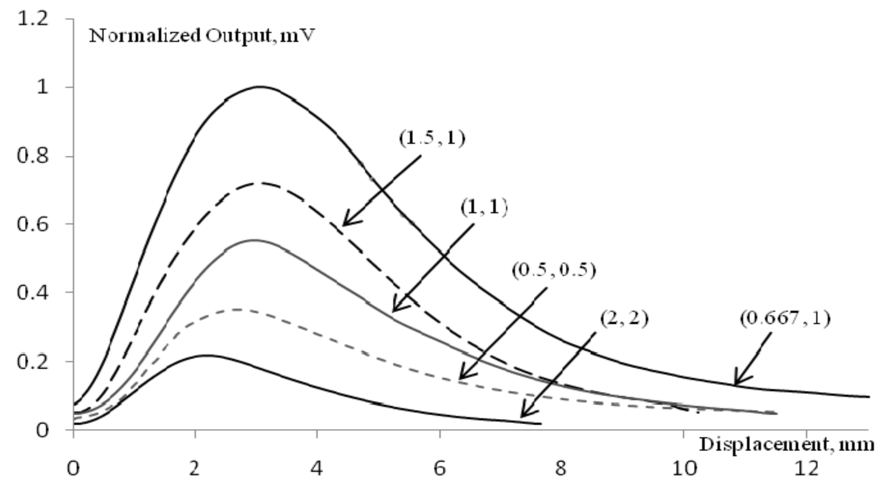

(a) at 20° angle

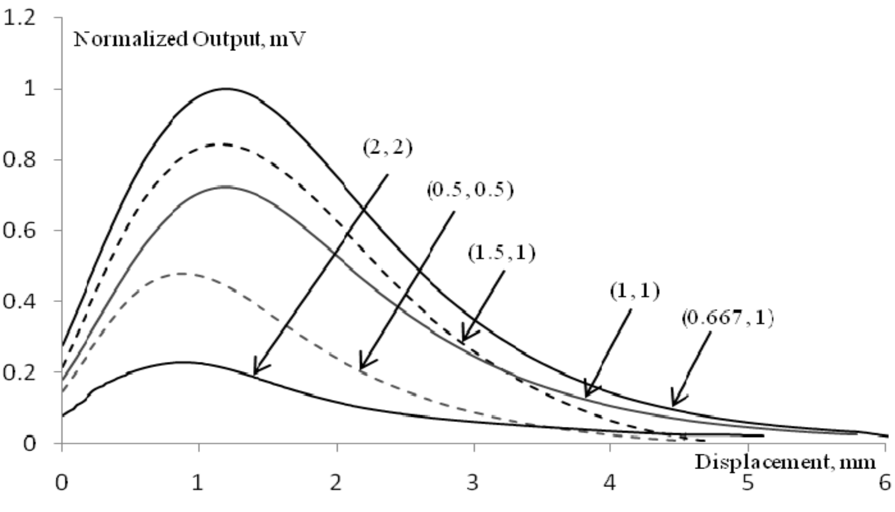

(c) at 30° angle

Fig. 5. The normalized output power against displacement for the FODS at various k_1 and k_2 values with different inclination angles (a) 10°; (b) 20° and (c) 30°.

Table 1. Summary of performances for the proposed FODS.

Methods	Front slopes						Back slopes					
	Sensitivity (mV/µm)			Linearity Range (mm)			Sensitivity (mV/µm)			Linearity Range		
(k_1, k_2)	10°	20°	30°	10°	20°	30°	10°	20°	30°	10°	20°	30°
(0.5, 0.5)	0.1345	0.1838	0.4761	1.5-3.5	0.4-2.1	0-0.7	0.0223	0.0479	0.1447	4.3-11.5	2.9-8.9	1.5-3.7
(0.667, 1)	0.2752	0.3759	0.7286	1 – 5.2	0.1-2.8	0 - 1	0.0675	0.1336	0.3224	6.6-17	3.2-10.2	1.3-4.3
(1, 1)	0.1671	0.2224	0.5528	1.2-4.8	0.2-2.8	0 - 1	0.0472	0.0823	0.2296	5.6-14.8	3 - 9	1.2-4.3
(1.5, 1)	0.1885	0.2745	0.6371	1.2-4.8	0.1-2.9	0 - 1	0.056	0.1155	0.2929	6.8-16	3.2-9.2	1.2-4.3
(2, 2)	0.0645	0.1201	0.1904	1.4-3.5	0.2- 2	0-0.8	0.0128	0.0389	0.0885	4.5-11.5	2.4-7.5	1 - 3

The same experiments are carried out using a liquid as a medium between probe and reflector by fixing the inclination angle at 10°. The results obtained are shown in Fig. 6 for three different liquids; liquid isopropyl alcohol, water and methanol. The isopropyl alcohol, water and methanol have a refractive index n value of 1.3772, 1.333 and 1.329, respectively. In the experiment, the k_1 and k_2 values are fixed at 2 and 2, respectively while the room temperature is set at around 25° to decrease the measurement errors. As shown in Fig. 6, the output power collected by the sensor reduces at small distance (< 2 mm) and increases at a longer distance, with the increment of refractive index. As the refractive index of the medium increases, the angle of emittance decreases hence output power collected decreases because of less overlapping area for displacement smaller than 2 mm. But after this distance density of reflected light increase so output intensity increases. As shown in Fig. 6, the LRIS produces the highest sensitivity at displacement about 3.3 mm. At this distance, the increment of intensity as the refractive index increases is the highest. The output intensity also increases almost linearly as a function of refractive index of the medium.

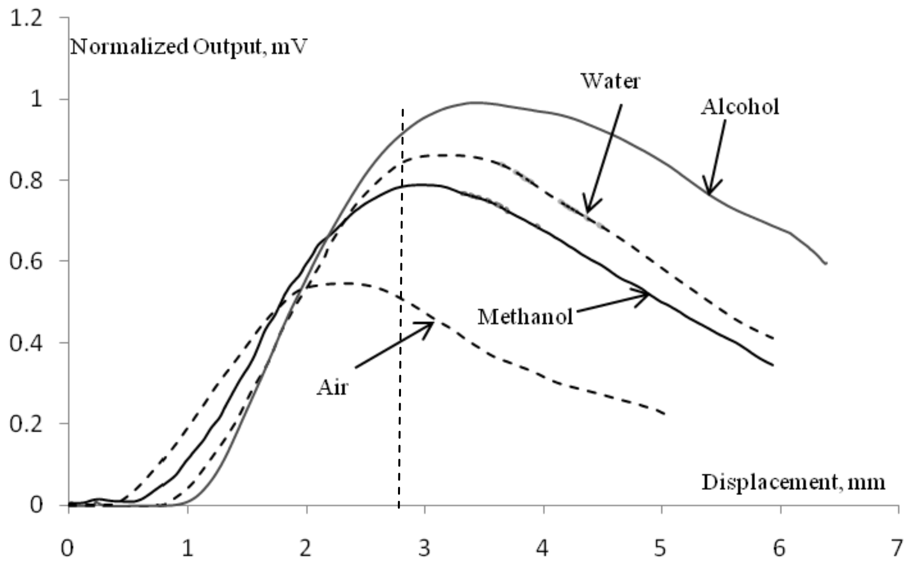

Fig. 6. Normalized output against displacement for the proposed LRIS at k_1, k_2 and angle values of (2, 2, 10°).

5. Conclusions

This paper presents the FODS and LRIS using two asymmetrical inclined transmitting and receiving fibers. A mathematical model based on optical geometry is proposed. The theoretical result of the FODS is in good agreement with the experimental result, verifying the feasibility of this theoretical model. The performance of FODS is strongly depended on the core radius and diameter of transmitting and receiving fibers as well as the inclination angle. The maximum sensitivities of 0.2752 mV/μm, 0.3759 mV/μm and 0.7286 mV/μm are obtained at inclination angles of 10°, 20° and 30°, respectively for the proposed FODS. Meanwhile, the maximum linear ranges of 10.4 mm, 7 mm and 3mm are obtained at inclination angles of 10°, 20° and 30°, respectively. For the LRIS, the output intensity increases almost linearly as a function of refractive index of the medium at displacement angle of 3.3 mm.

References

[1]. P. K. Rastogi, Optical Measurement Techniques and Applications, *Artech House, Inc*., Boston, London, 1997.

[2]. J. B. Faria, A theoretical analysis of the bifurcated fiber bundle displacement sensor, *IEEE Transactions on instrumentation and measurement*, Vol. 47, 1998, pp. 742-747.

[3]. H. M. Cao, Y. P. Chen, Z. D. Zhou, G. Zhang, Theoretical and experimental study on the optical fiber bundle displacement sensors, *Sensor and Actuators A,* Vol. 136, 2007, pp. 580-587.

[4]. P. B. Buchade and A. D. Shaligram, Simulation and experimental studies of inclined two fiber displacement sensor, *Sensor and Actuators A,* Vol. 128, 2006, pp. 312- 316.

[5]. P. B. Buchade and A. D. Shaligram, Influence of fiber geometry on the performance of two-fiber displacement sensor, *Sensor and Actuators A*, Vol. 136, 2007, pp. 199- 204.

[6]. F. E. Utou, J. Gryzagoridis and B. Sun, Parameters affecting the performance of fiber optic displacement sensors, *Smart Mater. Struct.,* Vol. 15, 2006, pp. 154-157.

[7]. B. E. Nottingk, Instrumentation Reference Book, 2nd Edition, *Butterworths*, London, 1995.

[8]. V. Kleizal and J. Verkelis, Some Advanced Fiber-Optic Amplitude Modulated Reflection Displacement and Refractive Index Sensors, *Nonlinear Analysis: Modeling and Control*, Vol. 12, No. 2, 2007, pp. 213–225.

[9]. P. Nath, H. K. Singh, P. Datta and K. C. Sarma, All-fiber optic sensor for measurement of liquid refractive index, *Sensor and Actuators A,* Vol. 148, 2008, pp. 16-18.

2009 Copyright ©, International Frequency Sensor Association (IFSA). All rights reserved.
(http://www.sensorsportal.com)